

# Transition Metal-Free Catalytic C–H Zincation and C–H Alumatation

Milan Kumar Bisai<sup>a‡</sup>, Justyna Łosiewicz<sup>a‡</sup>, Lia Sotorrios<sup>b</sup>, Gary S. Nichol<sup>a</sup>, Andrew P. Dominey<sup>d</sup>, Michael J. Cowley<sup>a</sup>, Stephen P. Thomas<sup>a</sup>, Stuart A. Macgregor<sup>b,c\*</sup> and Michael J. Ingleson<sup>a\*</sup>

<sup>a</sup> EaStCHEM School of Chemistry, University of Edinburgh, Edinburgh, EH9 3FJ, United Kingdom

<sup>b</sup> Institute of Chemical Sciences, Heriot-Watt University, Edinburgh, EH14 4AS, United Kingdom

<sup>c</sup> EaStCHEM School of Chemistry, University of St Andrews, KY16 9ST, United Kingdom

<sup>d</sup> GSK Medicines Research Centre, Gunnels Wood Road, Stevenage, Hertfordshire SG1 2NY, United Kingdom

**ABSTRACT:** C–H metalation is the most efficient method to prepare aryl–zinc and –aluminum complexes that are highly useful nucleophiles. Virtually all C–H metalation routes to form Al or Zn organometallic reagents require stoichiometric, strong Brønsted bases with no base-catalyzed reactions reported, to our knowledge. Herein we present a catalytic C–H metalation process to form aryl–zinc and aryl–aluminum complexes that uses only simple amine bases (e.g., Et<sub>3</sub>N) in sub-stoichiometric quantity (10 mol%). Key to this approach is coupling an endergonic C–H metalation step using a  $[(\beta\text{-diketimate})\text{M}-\text{NR}_3]^+$  (M = Zn or Al–Me) electrophile with a sufficiently exergonic dehydrocoupling step between the acidic ammonium salt by-product of C–H metalation ( $[(\text{R}_3\text{N})\text{H}]^+$ ) and a Zn–H or Al–Me containing complex. This step, forming H<sub>2</sub>/MeH, makes the overall cycle exergonic while also generating more of the key cationic metal electrophile. Mechanistic studies supported by DFT calculations revealed metal-specific dehydrocoupling pathways, with the divergent reactivity shown to be due to the different metal valency (which impacts the accessibility of amine-free cationic complexes) and steric environment. Notably, dehydrocoupling in the zinc system proceeds through a ligand-mediated pathway involving protonation of the  $\beta$ -diketimate C<sub>γ</sub> position. In this step the magnitude of the key barrier is dependent on the steric bulk of the spectator ligand, with bulkier ligands actually affording lower barriers. This catalytic approach to arene C–H metalation has the potential to be applicable to other main group metals and ligands, thus will facilitate the synthesis of these important organometallic compounds.

Catalyzed C–H functionalization is ubiquitous in synthesis as it is a highly efficient way to increase molecular complexity.<sup>1</sup> In this field, (hetero)arene C–H borylation using transition metal catalysts is particularly powerful,<sup>2</sup> while catalytic C–H silylation has also been developed into a useful synthetic tool (Fig. 1a).<sup>3</sup> In comparison, catalytic (hetero)arene C–H functionalization processes that install more electropositive main group elements are extremely under-developed.<sup>4</sup>

Zinc- and aluminum-based organometallics are desirable to form as they are more nucleophilic than organo-boranes/-silanes and are widely used in synthesis,<sup>5</sup> with arylzinc reagents ubiquitous due to the Negishi cross-coupling reaction.<sup>6</sup> Furthermore, both zinc and aluminum are Earth-abundant metals with high permitted daily exposure limits.<sup>7</sup> To date, methods that convert C–H bonds directly into C–Zn and C–Al bonds are dominated by the use of at least one equivalent of a strong Brønsted base combined with a zinc/ aluminum electrophile (Fig. 1b).<sup>8,9</sup> In contrast to stoichiometric methods, catalytic C–H zincation/alumination is extremely rare despite the higher efficiency of this approach (Fig. 1c) relative to stoichiometric (in base) processes. To our knowledge the only reports on catalytic (hetero)arene C–H zincation and C–H aluminination use a ( $\beta$ -diketiminato)ZnH<sup>10</sup> and a ( $\beta$ -diketiminato)AlH<sub>2</sub>,<sup>11</sup> respectively, as the starting materials, with H<sub>2</sub> formed as the only by-product. Pd catalysis was crucial in these processes as < 5% C–H metalation is observed in the absence of a Pd catalyst. Notably, transition metal-free catalytic C–H zincation/alumination has not been reported to our knowledge, despite this representing an attractive addition to established methods.

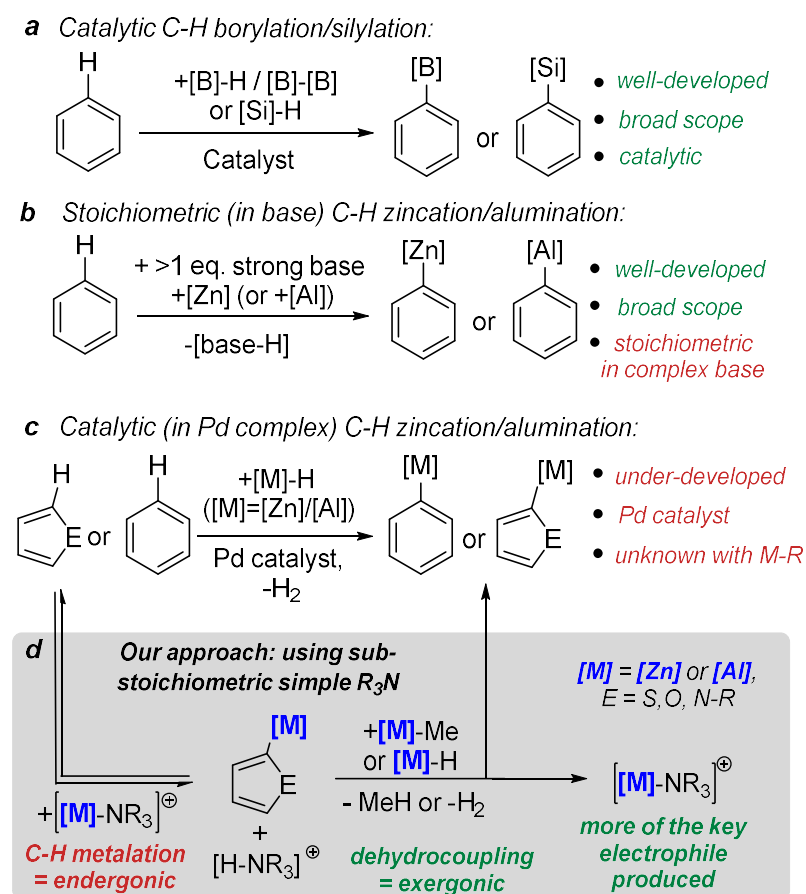


**Figure 1.** (a) Catalytic C–H borylation/silylation. (b) C–H zincation/alumination using stoichiometric base. (c) Catalytic C–H zincation/alumination using a Pd-catalyst. (d) This work, catalytic in amine heteroaryl C–H zincation and C–H aluminination.

In developing new Al/Zn catalytic C–H metalation routes, it is instructive to consider the more established area of catalytic C–H borylation. In transition metal-free C–H borylation reactions frustrated Lewis pairs (FLPs) are often used to effect C–H functionalization.<sup>12</sup> During this process an electrophilic borane forms the C–B bond while a basic component (e.g., R<sub>3</sub>N) is protonated. The resultant Brønsted acid (e.g., [(R<sub>3</sub>N)H]<sup>+</sup>) then can react with a hydroborane forming H<sub>2</sub> (termed dehydrocoupling herein). This step can enable the process to be catalytic as it can regenerate the reactive boron electrophile and the base. With the correct borane and base both the C–H borylation and dehydrocoupling steps are exergonic.<sup>13</sup> Any analogous chemistry using Zn or Al electrophiles must overcome the problem of weaker (vs. C–B) C–Zn and C–Al bonds, which results in the crucial C–H metalation step being endergonic. Building on studies using Zn- and Al-based FLPs,<sup>14</sup> we postulated that combining an endergonic FLP-mediated C–H metalation step with a subsequent exergonic dehydrocoupling step (between [(Base)H]<sup>+</sup> and [Zn]–H/[Al]–H) would lead to an overall exergonic process. With correctly designed systems this would enable catalytic (sub-stoichiometric in base) C–H metalation as more of the key electrophilic metal complex will be formed post dehydrocoupling (e.g., Fig. 1d). Precedence for this approach is extremely limited, with a study from Roesky and co-workers on the alumination of two activated *N*-heterocycles using an FLP the closest relevant work.<sup>15</sup> Their calculations indicated that dehydrocoupling was key to the overall reaction being exergonic (Fig. 2, top). While this process is stoichiometric (in hindered base), it indicated that transition metal-free catalytic C–H metalation is feasible provided the energetics of C–H metalation and dehydrocoupling are appropriate.

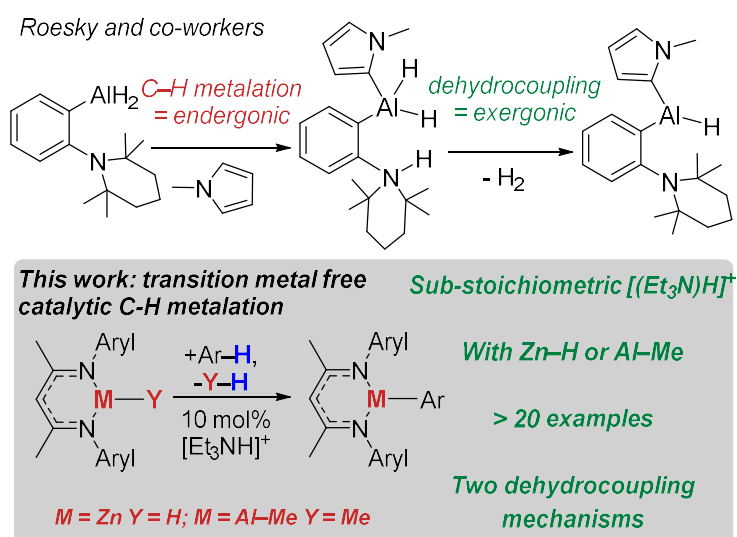


**Figure 2.** Top: Previous work on [Al]-FLP-mediated C–H alumination. Bottom: [Zn]/NR<sub>3</sub> and [Al]/NR<sub>3</sub> C–H metalation using sub-stoichiometric [(R<sub>3</sub>N)H]<sup>+</sup>.

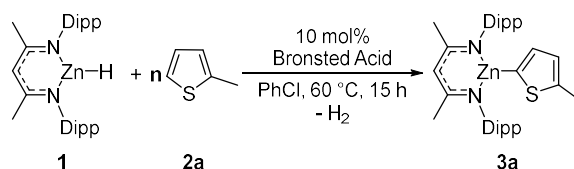
Herein we report that sub-stoichiometric quantities of simple amines (added as ammonium salts) enable the catalytic C–H zincation/alumination of heteroarenes using metal hydrides/alkyls (Fig. 2 bottom) with H<sub>2</sub>/MeH the only by-product. Notably, the dehydrocoupling step in the C–H zincation process is only feasible due to ligand non-innocence. Combined, this work introduces a transition metal-free, catalytic approach to make C–Zn and C–Al bonds directly from the heteroarene.

## RESULTS AND DISCUSSION

### C–H Zincation Studies

As part of our recent C–H borylation work we demonstrated that the reaction of  $\text{NacNacZnH}$  ( $\text{NacNac} = \{(2,6\text{-}^i\text{Pr}_2\text{C}_6\text{H}_3)\text{N}(\text{CH}_3)\text{C}\}_2\text{CH}$ ) with an anilinium cation,  $[(\text{DMT})\text{H}]^+$  ( $\text{DMT} = N,N\text{-dimethyl-4-toluidine}$ ), to form  $\text{H}_2$  and  $[\text{NacNacZn}(\text{DMT})]^+$  is exergonic.<sup>14c</sup> Initial computational studies indicated that  $\text{DMT}$  can be displaced from zinc by a heteroarene. The resultant  $\text{Zn}$ -(heteroaryl-H) complex and free  $\text{DMT}$  were then calculated to effect C–H zincation with feasible barriers (for solution reactivity). While this FLP-type C–H zincation was calculated to be significantly endergonic, coupling it with a dehydrocoupling step (between  $\text{NacNacZnH}$  (**1**) and  $[(\text{DMT})\text{H}]^+$ ) was explored as a route to make the C–H zincation process exergonic overall. Initially, **1** and equimolar 2-methyl-thiophene, **2a** (selected as the model substrate given its propensity to undergo C–H borylation using boron-based FLPs),<sup>12</sup> were combined with 10 mol%  $[(\text{DMT})\text{H}][\text{B}(\text{C}_6\text{F}_5)_4]$ . This led to 41% conversion to the C–H zincation product **3a** after heating at 60 °C for 15 h in chlorobenzene ( $\text{PhCl}$ , Table 1, entry 1). Under identical conditions in the absence of the ammonium salt no C–H metalation was observed (entry 2).

**Table 1.** C–H zincation of 2-methyl-thiophene.<sup>a</sup>



	Brønsted Acid	n	Yield (%) <sup>b</sup>
<b>1</b>	$[(\text{DMT})\text{H}][\text{B}(\text{C}_6\text{F}_5)_4]$	1	41
<b>2</b>	-	1	0
<b>3</b>	$[(\text{DMT})\text{H}][\text{B}(\text{Ar}^{\text{CF}_3})_4]$	1	45
<b>4</b>	$[(\text{Et}_3\text{N})\text{H}][\text{B}(\text{Ar}^{\text{CF}_3})_4]$	1	68
<b>5</b>	$[(\text{Et}_3\text{N})\text{H}][\text{B}(\text{C}_6\text{F}_5)_4]$	1	60
<b>6</b>	$[(\text{DET})\text{H}][\text{B}(\text{C}_6\text{F}_5)_4]$	1	31
<b>7</b>	$[2,4\text{-Br}_2\text{C}_6\text{H}_3\text{-NMe}_2\text{H}][\text{B}(\text{C}_6\text{F}_5)_4]$	1	14
<b>8</b>	$[(\text{Ph}_3\text{P})\text{H}][\text{B}(\text{C}_6\text{F}_5)_4]$	1	0
<b>9</b>	$[(\text{Et}_3\text{N})\text{H}][\text{OTf}]$	1	0
<b>10</b>	$[(\text{DMT})\text{H}][\text{OTf}]$	1	0
<b>11</b>	$[(\text{DMT})\text{H}][\text{NTf}_2]$	1	0
<b>12</b>	$[(\text{Et}_3\text{N})\text{H}][\text{B}(\text{Ar}^{\text{CF}_3})_4]$	2	78
<b>13</b>	$[(\text{Et}_3\text{N})\text{H}][\text{B}(\text{Ar}^{\text{CF}_3})_4]$	3	87
<b>14<sup>c</sup></b>	$[(\text{Et}_3\text{N})\text{H}][\text{B}(\text{Ar}^{\text{CF}_3})_4]$	2	88
<b>15<sup>d</sup></b>	$[(\text{Et}_3\text{N})\text{H}][\text{B}(\text{Ar}^{\text{CF}_3})_4]$	2	82

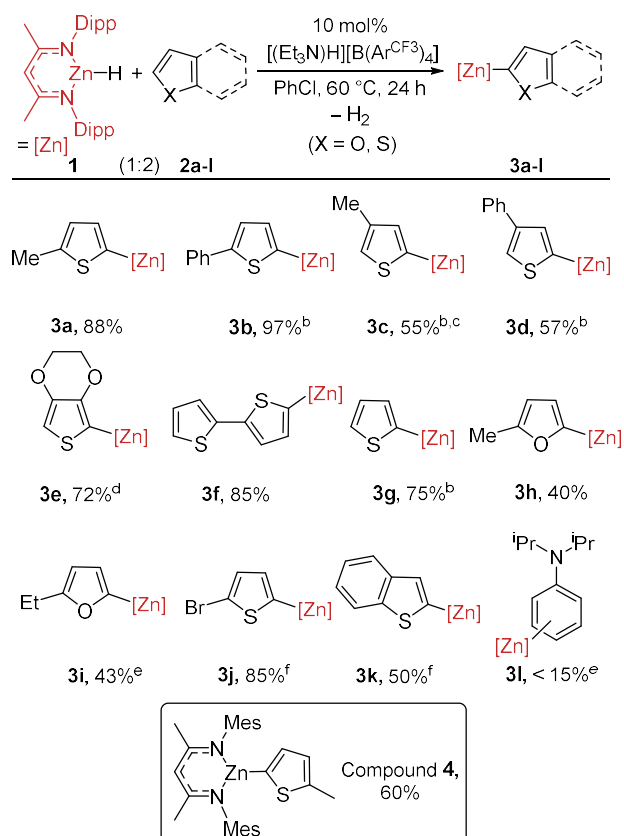
<sup>a</sup> **1** (0.1 mmol, 1.0 equiv.), **2a** (n equiv.), and Brønsted acid (0.01 mmol, 0.1 equiv) in  $\text{PhCl}$  (0.6 mL). <sup>b</sup> Yield by  $^1\text{H}$  NMR spectroscopy versus  $\text{CH}_2\text{Br}_2$  added as internal standard at the end. <sup>c</sup> Reaction carried out for 24 h. <sup>d</sup> Reaction carried out at 70 °C.

With the feasibility of catalytic C–H zincation confirmed, we screened several other Brønsted acidic salts. From this, better conversions were achieved using [(Et<sub>3</sub>N)H]<sup>+</sup> salts, while there was minimal difference switching between the two fluorinated aryl-borate anions (entries 1, 3-5, B(Ar<sup>CF<sub>3</sub></sup>)<sub>4</sub> = B{3,5-C<sub>6</sub>H<sub>3</sub>(CF<sub>3</sub>)<sub>2</sub>})<sub>4</sub>). Et<sub>3</sub>N is more basic and bulkier than DMT (pK<sub>a</sub> [(DMT)H]<sup>+</sup> = 10.8, [(Et<sub>3</sub>N)H]<sup>+</sup> = 18.5, all pK<sub>a</sub>'s are in acetonitrile)<sup>16</sup>. From reactions using two other ammonium salts and a phosphonium salt (entries 6-8, DET = *N,N*-diethyl-4-toluidine, [(DET)H]<sup>+</sup> pK<sub>a</sub> = 14.2, [2,4-Br<sub>2</sub>C<sub>6</sub>H<sub>3</sub>-NMe<sub>2</sub>H]<sup>+</sup> pK<sub>a</sub> = 8.3, [(Ph<sub>3</sub>P)H]<sup>+</sup> pK<sub>a</sub> = 7.14) we found using the conjugate acid of a base that is both bulky and highly Brønsted basic leads to more effective catalytic C–H zincation. Robust, weakly coordinating anions, such as the fluorinated borates are essential, since more coordinating anions ([OTf]<sup>-</sup> and [NTf<sub>2</sub>]<sup>-</sup>) inhibit the catalytic process (entries 9-11). Finally, using two equivalents of heteroarene, and slightly longer reaction times led to the yield of the C–H zincation product **3a** improving to 88% (entry 12-15). This demonstrates for the first time that C–H zincation catalytic in simple base is feasible and can be high yielding.

Subsequently, we surveyed a range of heteroarenes in this C–H zincation process (Table 2). Replacement of Me with Ph on thiophene led to **3b** forming in 97% yield. C3-Substituted thiophenes also were amenable, producing **3c** and **3d**. While 3-methyl-thiophene gave both 2-zincated and 5-zincated products (in 16% and 55% yield, respectively), the bulkier 3-phenyl derivative produced only the single isomer shown. The more nucleophilic thiophene 3,4-ethylenedioxy-thiophene underwent faster C–H zincation and gave **3e** in 72% yield within 1 h. 2,2'-Bithiophene and thiophene also underwent regioselective α C–H zincation to form **3f** and **3g** in good yield. This zincation methodology also could be applied to furans to provide C–H zincation products **3h-3i** in moderate yield, with unreacted starting material making up the mass balance. Pleasingly, even the significantly less activated heteroarenes 2-Br-thiophene and benzothiophene (Mayr *N* value = -2.6)<sup>17</sup> were amenable, although C–H zincation required a higher temperature for good conversion to **3j** and **3k**. Note, the benzothiophene C2 and C3 positions have similar reactivity in S<sub>E</sub>Ar, with C2 substitution leading to the thermodynamic product (note, an analogous outcome was observed in electrophilic C–H borylation).<sup>18</sup> Attempts to C–H zincate *N*-Me-pyrrole and *N*-Me-indole did appear to proceed, however, conversions were always < 40% and sufficiently clean samples to permit unambiguous characterization of the products could not be obtained.

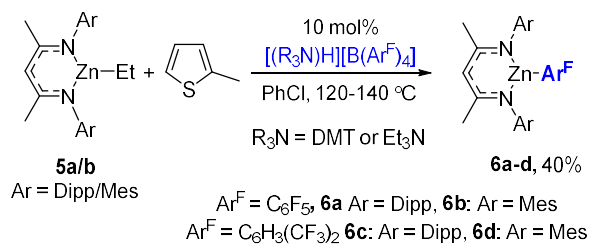
An *N,N*-disubstituted aniline derivative led to minimal reaction (e.g. < 15% of a compound tentatively assigned as **3l**) even after prolonged heating. Furthermore, there was no C–H zincation of haloarenes, including those with relatively low pK<sub>a</sub> values (e.g., C<sub>6</sub>F<sub>5</sub>H) in contrast to the Pd-catalyzed process.<sup>10</sup> Thus, this C–H zincation is dependent on heteroarene nucleophilicity and not heteroarene *pK<sub>a</sub>*, consistent with an S<sub>E</sub>Ar-type mechanism.

Next, another NacNac ligand was explored, the smaller *N*-mesityl derivative, <sup>Mes</sup>NacNacZnH. Using this led to 60% of the zincation product, **4** (inset bottom Table 2) under the standard conditions. Monitoring the reaction *in-situ* revealed it was slower than the zincation of 2-methyl-thiophene using **1**, presumably due (at least in part) to the lower solubility of <sup>Mes</sup>NacNacZnH in PhCl (relative to the <sup>Dipp</sup>NacNac congener). We would note that NacNacZn-Aryl complexes have been shown previously by Crimmin and co-workers to be effective sources of aryl nucleophiles in Negishi cross-coupling and in allylation reactions.<sup>10</sup>

**Table 2.** Scope of C–H zincination of heteroarenes.<sup>a</sup>

<sup>a</sup> **1** (0.1 mmol), **2a-l** (0.2 mmol), and  $[(Et_3N)H][B(Ar^{CF_3})_4]$  (0.01 mmol) in PhCl (0.6 mL) at 60 °C for 24 h unless otherwise stated. Yield by <sup>1</sup>H NMR spectroscopy versus  $CH_2Br_2$  added as an internal standard at the end of the reaction. <sup>b</sup> at 80 °C for 24 h. <sup>c</sup> 16% zincination at C-2 position also was observed. <sup>d</sup> at 60 °C for 1 h. <sup>e</sup> at 80 °C for 48 h. <sup>f</sup> at 100 °C for 24 h.

The feasibility of using  $NacNacZnEt$  in place of the zinc hydride **1** also was explored, targeting a “transfer zincation” (Scheme 1) related to the recently reported catalyzed transfer borylation.<sup>19</sup> However, no zincination of 2-methylthiophene was observed with either the *N*-Dipp or *N*-Mes derivatives (**5a/b**) using 10 mol% of several ammonium salts. At  $\geq 120$  °C the formation of  $NacNacZnAr^F$  (**6a-d**,  $Ar^F = C_6F_5$  or  $3,5-C_6H_3(CF_3)_2$ ) in *ca.* 40% yield was observed, from decomposition of the anion (see Fig. S71-S78). This is likely due to the decomposition of a species such as  $[NacNacZn-NR_3][B(Ar^F)_4]$  at  $\geq 120$  °C as  $[(R_3N)H][B(Ar^F)_4]$  salts are stable under these conditions.

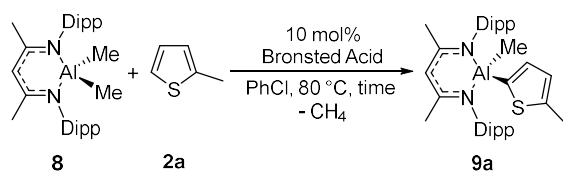
**Scheme 1.** Attempted C–H zincination with  $NacNacZnEt$ .

## C–H Almination Studies

With an effective C–H zincation process in hand we explored the feasibility of extending this approach to another main group metal. Aluminum was selected partly due to the factors discussed in the introduction, but also as aluminum is distinct from zinc in multiple ways (particularly in valency and coordination number of the  $\text{NacNacM-R}_{1/2}$  complexes). If the same approach of coupling endergonic C–H metalation (using a  $[\text{Al}]-\text{NR}_3$  cation in this case) with exergonic dehydrocoupling also was successful with Al it would indicate broad (in terms of metal) scope.

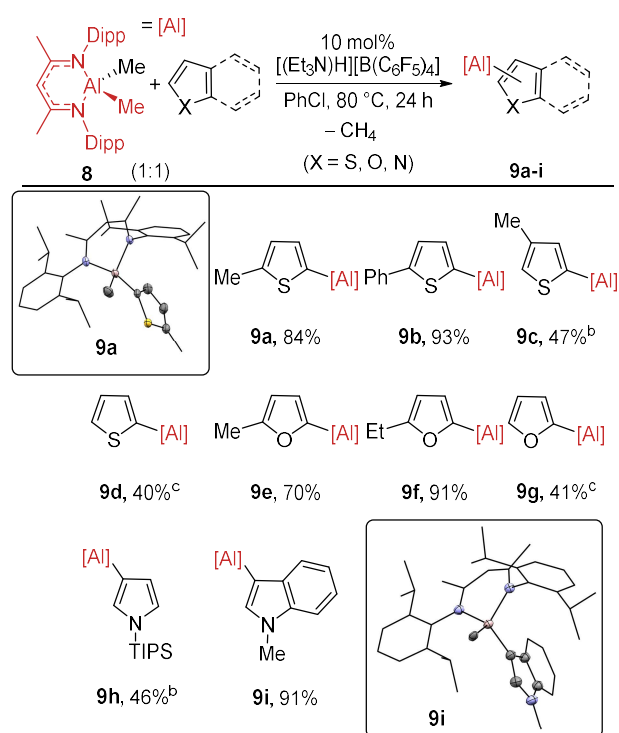
Initial attempts using  $\text{NacNacAlH}_2$  (**7**) in place of the zinc-hydride led to the formation of complex intractable mixtures. Therefore, the use of  $\text{NacNacAlMe}_2$  (**8**) was explored in place of **7**. While  $\text{NacNacZnEt}$  was not viable in C–H metalation, we hypothesized that the greater polarization of  $\text{Al-C}_{\text{alkyl}}$  bonds, relative to  $\text{Zn-C}_{\text{alkyl}}$  (based on  $\Delta\chi$  between M and C)<sup>20</sup> could lead to a lower barrier in any Al–alkyl protonolysis step. Pleasingly, the catalytic C–H metalation of **2a** using **8** and 10 mol%  $[(\text{Et}_3\text{N})\text{H}][\text{B}(\text{C}_6\text{F}_5)_4]$  proceeded cleanly to give aryl aluminum **9a** as the major product on heating to 80 °C (Table 3, entry 1). Importantly, in the absence of  $[(\text{Et}_3\text{N})\text{H}][\text{B}(\text{C}_6\text{F}_5)_4]$  no C–H almination was observed (entry 2). This process thus represents the first report of catalytic transfer almination. A comparison study then was performed using the two  $[(\text{R}_3\text{N})\text{H}][\text{Anion}]$  salts that performed best as activators in C–H zincation. With **8**, better conversions were again achieved using  $[(\text{Et}_3\text{N})\text{H}][\text{B}(\text{C}_6\text{F}_5)_4]$  compared to the  $[(\text{DMT})\text{H}]^+$  salt. The poor performance of salts with  $[\text{B}(\text{Ar}^{\text{CF}_3})_4]^-$  anions (entry 4 and 5) in this case is notable, with *in-situ* reaction monitoring revealing the formation of several new fluorinated compounds (by <sup>19</sup>F NMR spectroscopy). The difference in C–H almination using  $[\text{B}(\text{Ar}^{\text{CF}_3})_4]^-$  and  $[\text{B}(\text{C}_6\text{F}_5)_4]^-$ , is consistent with the considerable fluorophilicity of aluminum cations that presumably leads to Al–F bond formation by fluoride abstraction from the  $\text{sp}^3\text{-CF}_3$ -containing anion (note, this is not observed with the zinc congeners at 80 °C, consistent with the lower fluorophilicity of Zn relative to Al).

**Table 3.** C–H almination of 2-methyl-thiophene.<sup>a</sup>



Entry	Brønsted Acid	Time (h)	Yield (%) <sup>b</sup>
1	$[(\text{Et}_3\text{N})\text{H}][\text{B}(\text{C}_6\text{F}_5)_4]$	20	80
2	-	18	0
3	$[(\text{DMT})\text{H}][\text{B}(\text{C}_6\text{F}_5)_4]$	20	54
4	$[(\text{DMT})\text{H}][\text{B}(\text{Ar}^{\text{CF}_3})_4]$	20	0
5	$[(\text{Et}_3\text{N})\text{H}][\text{B}(\text{Ar}^{\text{CF}_3})_4]$	20	0
6	$[(\text{Et}_3\text{N})\text{H}][\text{B}(\text{C}_6\text{F}_5)_4]$	24	84

<sup>a</sup> **8** (0.1 mmol), **2a** (0.1 mmol) and Brønsted acid (0.01 mmol) in  $\text{PhCl}$  (0.6 mL). <sup>b</sup> Yield by <sup>1</sup>H NMR spectroscopy versus  $\text{CH}_2\text{Br}_2$  added as an internal standard at the end.

**Table 4.** Scope of C–H alumination of heteroarenes.<sup>a</sup>

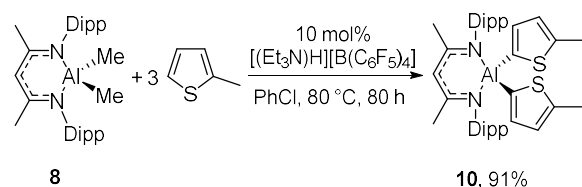
<sup>a</sup> **8** (0.1 mmol), heteroarene (0.1 mmol), and ammonium salt (0.01 mmol) in PhCl (0.6 mL) at 80 °C for 24 h. Yield by <sup>1</sup>H NMR spectroscopy versus CH<sub>2</sub>Br<sub>2</sub> added as an internal standard. <sup>b</sup> at 80 °C for 48 h. <sup>c</sup> at 100 °C for 24 h.

To determine the scope of this catalytic C–H alumination methodology, a range of heteroarenes was explored (Table 4). Similar to observations from C–H zincation, 2-substituted thiophenes (to form alumination products **9a** and **9b**) and 3-substituted thiophenes (forming **9c**) were amenable to C–H alumination. In this case, 3-methyl-thiophene underwent regioselective C–H alumination to provide only the 5-substituted product, **9c**, in contrast to the zinc system where both  $\alpha$ -metalated isomers are formed.  $\alpha$ -Selective C–H alumination was confirmed for **9a** by single-crystal X-ray diffraction studies (inset top Table 4). This C–H alumination process also was applicable to thiophene, although its lower nucleophilicity<sup>17</sup> meant higher reaction temperatures were required. The less activated heteroarenes 2-Br-thiophene and benzothiophene did not undergo any C–H alumination at 100 °C. These observations are again consistent with an S<sub>E</sub>Ar-type mechanism. The absence of C–H alumination for the two less nucleophilic heteroarenes indicates a higher turnover limiting barrier for these two substrates with aluminum relative to the zinc system. Nevertheless, catalytic C–H alumination worked well for O/N-containing activated heterocycles. For example, furans showed good reactivity (forming **9e-g**), while C–H functionalization of *N*-TIPS-pyrrole proceeded at the C3-position in moderate yield (46% **9h**, in 48 h). *N*-Me-indole underwent selective C–H alumination at the most nucleophilic C3-position to give an excellent (91%) yield of the product, **9i**. The formation of the C3-metalated isomer **9i** was confirmed by single crystal X-ray diffraction studies (inset bottom Table 4). The C3 functionalization of *N*-Me-indole under these conditions is also consistent with an S<sub>E</sub>Ar-type process and is in contrast to the C–H alumination of *N*-Me-indole under the previously reported Pd-catalyzed conditions which proceeded selectively at the C-2 position.<sup>11</sup> This further highlights the distinct mechanisms of these two catalytic C–H alumination methodologies. It also should be noted that a range of phenyl

derivatives, e.g. *N,N*-diisopropylaniline, again underwent minimal (or no) C–H aluminination using our approach as per the zinc system. Again, we would note that Crimmin and co-workers have shown previously that *NacNacAl*-(R)Aryl complexes are useful sources of aryl nucleophiles in Nickel catalyzed cross coupling reactions with aryl bromides.<sup>11c</sup>

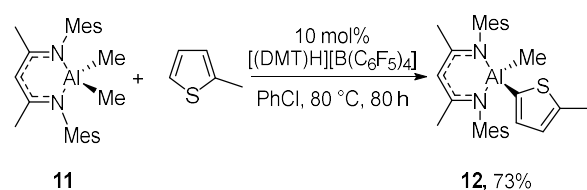
Next, we sought to functionalize both the aluminum-methyl groups in *NacNacAlMe*<sub>2</sub> (**8**) by increasing the number of equivalents of heteroarene used (from 1 equiv. in the reactions in Table 4). The reaction of **8** with 3 equiv. of 2-methylthiophene in the presence of 10 mol% [(Et<sub>3</sub>N)H][B(C<sub>6</sub>F<sub>5</sub>)<sub>4</sub>] yielded 91% double C–H aluminination product **10** after 80 h (Scheme 2). Compound **10** was characterized by multinuclear and variable temperature NMR spectroscopy. It is noteworthy that a related *NacNacAl*(thienyl)<sub>2</sub> product was synthesized previously using the Pd-catalyzed C–H aluminination approach, however the Pd-catalyzed system required much more forcing conditions (200 °C).<sup>21</sup>

### Scheme 2. Double C–H aluminination.



This C–H metalation methodology again could be extended to the less sterically demanding <sup>Mes</sup>NacNac ligand. However, in contrast to the zinc system, for aluminum it required a change in the ammonium salt used. Specifically, 73% C–H aluminination of 2-methylthiophene with <sup>Mes</sup>NacNacAlMe<sub>2</sub> (**11**, Scheme 3) can be achieved to form **12** using 10 mol% [(DMT)H][B(C<sub>6</sub>F<sub>5</sub>)<sub>4</sub>]. In contrast, using 10 mol% [(Et<sub>3</sub>N)H][B(C<sub>6</sub>F<sub>5</sub>)<sub>4</sub>] and **11** / 2-methylthiophene led to a complex intractable mixture of products. This indicated that the right combination of *NacNacM* electrophile and amine base is essential for effective C–H metalation, with similar observations reported in other FLP-mediated reactions.<sup>12</sup>

### Scheme 3. C–H aluminination with a <sup>Mes</sup>NacNac derivative.



## Synthesis of cationic NacNacM electrophiles and solid-state structures

To gain insight into structure-reactivity relationships we synthesized a number of the NacNacZn salts starting from NacNacZnH and [(Base)H][Anion]. This afforded **13a-f** (Figure 3) as single products (by NMR spectroscopy). Given the importance to the catalytic process of forming **13** by dehydrocoupling with [(R<sub>3</sub>N)H]<sup>+</sup> (as the barrier to dehydrocoupling directly impacts  $\Delta G^{\ddagger}_{\text{span}}$ , *vide infra*) these reactions were monitored by *in-situ* NMR spectroscopy. This revealed that the more acidic cations, e.g. [(DMT)H]<sup>+</sup>, resulted in faster dehydrocoupling at room temperature compared to the [(Et<sub>3</sub>N)H]<sup>+</sup> salts (though these also react at room temperature), indicating a lower barrier to dehydrocoupling using [(DMT)H]<sup>+</sup>. No intermediates were observed during these protonolysis reactions. In contrast to the Zn–H congeners, the NacNacZnEt complexes **5a/5b** reacted with [(Et<sub>3</sub>N)H]<sup>+</sup> salts only at 50 °C and above, to form **13c, 13d** (from **5a**) and **13f** (from **5b**), with no reaction observed at room temperature. Thus, there is a higher barrier for ethane formation relative to H<sub>2</sub> formation in this system. This combined with endergonic C–H metalation (*vide infra*), explains the lack of heteroarene C–H zincation using the NacNacZnEt compounds **5a/b** at temperatures < 120 °C.

The solid-state structures of [NacNacZn(NEt<sub>3</sub>)] [B(Ar<sup>CF3</sup>)<sub>4</sub>] (**13c**), [<sup>Mes</sup>NacNacZn(NEt<sub>3</sub>)] [B(Ar<sup>CF3</sup>)<sub>4</sub>] (**13f**), and [NacNacZn(PPh<sub>3</sub>)] [B(C<sub>6</sub>F<sub>5</sub>)<sub>4</sub>] (**13e**) were determined (Figure 3B) and all found to contain three-coordinate trigonal planar zinc centers with effectively planar ( $\leq 0.05$  Å deviation) C<sub>3</sub>N<sub>2</sub>Zn metallacycles.<sup>22</sup> The Zn1–NEt<sub>3</sub> bond lengths are similar (**13c** = 2.008(4) Å and **13f** = 1.9945(13) Å) and as expected are longer than that in three-coordinate (at Zn) neutral NacNacZn–NR<sub>2</sub> complexes (where Zn–NR<sub>2</sub>  $\approx$  1.85 Å).<sup>23</sup> However, they are shorter compared to those in four coordinate [NacNacZn(amine)<sub>2</sub>]<sup>+</sup>,<sup>24</sup> and the TMEDAN–Zn distances in a three coordinate [(TMEDA)Zn–L]<sup>+</sup> cation.<sup>14e</sup> Combined, this data indicates minimal steric destabilization of the Zn–NEt<sub>3</sub> bonds in **13c** and **13f**.

In contrast to the systems containing [BAR<sup>F</sup>]<sup>–</sup> anions, reactions between NacNacZnH and [(DMT)H][OTf] afforded crystals of the dimeric complex {NacNacZn(μ–OTf)}<sub>2</sub>, **14** (Figure 3C). In this structure each OTf anion is bound to two zinc centers forming an eight-membered ring reminiscent of dimeric NacNacZn(carboxylate) derivatives.<sup>25</sup> *In-situ* NMR studies also revealed that DMT does not displace [OTf]<sup>–</sup> from zinc in **14** in solution (Fig. S142–S145). This suggests the poor outcomes using [OTf]<sup>–</sup> in the catalytic C–H zincation is due to the more coordinating nature of the [OTf]<sup>–</sup> anion toward zinc (relative to the [BAR<sup>F</sup>]<sup>–</sup> anions) which presumably blocks the heteroarene from interacting with the zinc center.

Stoichiometric reactions of NacNacAlMe<sub>2</sub> with [(Base)H][B(C<sub>6</sub>F<sub>5</sub>)<sub>4</sub>] also were performed. These afforded the cationic aluminum complexes cleanly for base = DMT and Et<sub>3</sub>N via methane elimination (Figure 3D). The protonolysis reactivity again correlates with the relative Brønsted acidity of the ammonium salts, with **15a** forming within 1 h at room temperature, while the Et<sub>3</sub>N derivative, **15b**, was formed fully only after heating for a prolonged period at 50 °C. No intermediates were observed during any of these protonolysis reactions.

The solid-state structure of [NacNacAl(Me)(DMT)] [B(C<sub>6</sub>F<sub>5</sub>)<sub>4</sub>], **15a** (Figure 3D), confirmed the formulation with the four coordinate aluminum center in a distorted tetrahedral geometry with metrics comparable to other four-coordinate NacNacAl(Me)-based complexes.<sup>26,27</sup> Steric effects in **15a** appear minimal as indicated by the Al–N<sub>DMT</sub> distance in **15a** (Al1–N3 2.010(6)) being comparable to that in other cationic four-coordinate Al–N(Ph)Me<sub>2</sub> complexes that have ligands with less bulky substituents.<sup>28</sup> As **15b** did not afford single crystals suitable for X-ray diffraction analysis, the structure of the cationic component was calculated (*vide infra* for detailed discussions of computational results). This

calculated structure possessed closely comparable metrics to the structure of **15a** indicating minimal differences to the geometry around aluminum on changing the amine from DMT to Et<sub>3</sub>N.

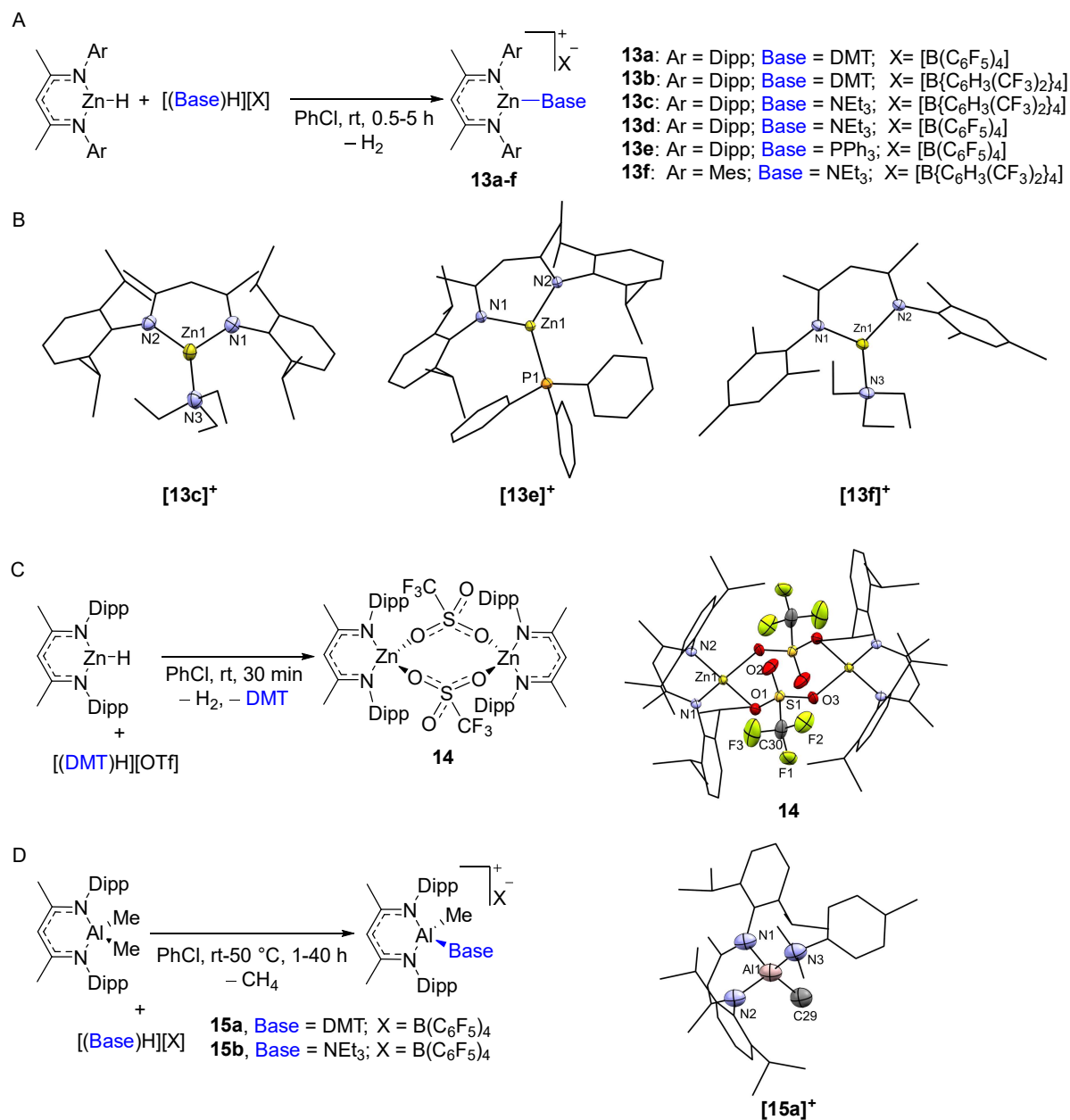
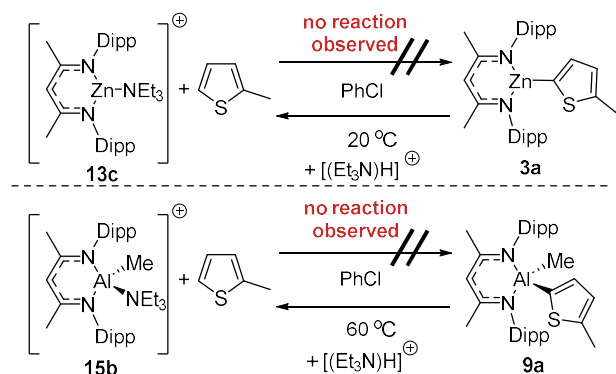


**Figure 3.** **A**, synthesis of **13a-f**. **B**, structures of the cationic components of **13c**, **e** and **f**. **C**, synthesis and structure of **14**. **D**, synthesis of **15a** and **15b** and structure of the cationic component of **15a**. Ellipsoids at 50% probability. Hydrogen atoms are omitted for clarity. Selected bond distances (Å) and angles (°) [**13c**]: Zn1–N1 1.921(4), Zn1–N2 1.897(4), Zn1–N3 2.008(4), N1–Zn1–N2 103.25(17), N2–Zn1–N3 134.37(17), N1–Zn1–N3 122.38(17); [**13e**]: Zn1–N1 1.9189(13), Zn1–N2 1.9055(12), Zn1–P1 2.3336(4), N1–Zn1–N2 102.48(5), N2–Zn1–P1 134.64(4), N1–Zn1–P1 122.26(4); [**13f**]: Zn1–N1 1.9010(12), Zn1–N2 1.8960(12), Zn1–N3 1.9945(13), N1–Zn1–N2 103.02(5), N2–Zn1–N3 130.41(5), N1–Zn1–N3 126.57(5); **14**: Zn1–N1 1.9433(17), Zn1–N2 1.9387(17), Zn1–O1 2.0072(16), Zn1–O3 2.054(2), S1–O1 1.4545(17), S1–O2 1.407(2), S1–O3 1.450(2); [**15a**]: Al1–N1 1.916(6), Al1–N2 1.907(6), Al1–N3 2.010(6), Al1–C29 1.932(7), N1–Al1–N2 96.9(3), N1–Al1–N3 113.2(3), N2–Al1–C29 112.4(3), C29–Al1–N3 107.3(3).

### Mechanistic Studies:

Firstly, the suspected endergonic nature of heteroarene C–H metalation using  $[\text{NacNacM-NEt}_3]^+$  ( $M = \text{Zn}/\text{Al-Me}$ ) cations was confirmed. For example, no change in the NMR spectra was observed upon addition of 20 equiv. of 2-methyl-thiophene to the zinc complex **13c** (at room temperature nor at 60 °C, Scheme 4 top). The subsequent addition of  $\text{NacNacZnH}$  (**1**) however still led to the C–H zincation of 2-methyl-thiophene at 60 °C. This is consistent with **1** reacting with  $[(\text{Et}_3\text{N})\text{H}]^+$  and thereby driving the C–H metalation forward. On complete consumption of **1** during catalytic C–H zincation compound **13c** again was observed, suggesting that it is an on-cycle species (Fig. S156). Analogous observations were forthcoming from the reaction of the aluminum complex **15b** and 2-methyl-thiophene (Scheme 4, bottom) e.g., no C–H metalation observed in the absence of  $\text{NacNacAlMe}_2$  (**8**) to scavenge the ammonium cation by-product from C–H metalation. Consistent with these observations the backwards reaction, i.e. protonolysis of the  $\text{NacNacM}$ -thienyl complexes **3a** and **9a** with  $[(\text{Et}_3\text{N})\text{H}]^+$ , proceeded to form 2-methyl-thiophene and **13c** and **15b**, respectively (Scheme 4 and Fig. S157-S158). Note, the reaction of **9a** with  $[(\text{Et}_3\text{N})\text{H}]^+$  to form **15b** was slightly slower than the reaction of **8** with  $[(\text{Et}_3\text{N})\text{H}]^+$  to form **15b**, indicating a higher barrier for the protonolysis of the Al-thienyl unit in **9a** group relative to the Al–Me unit in **8**.

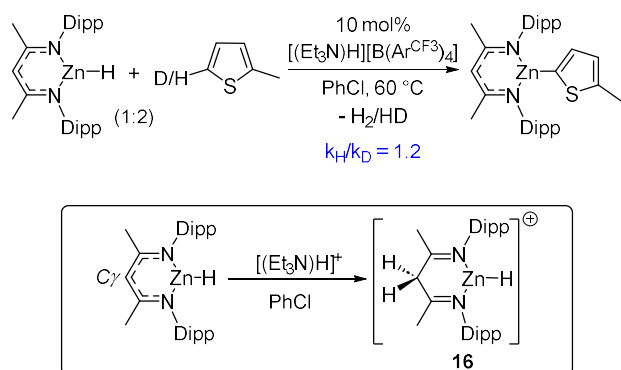
**Scheme 4.** Endergonic 2-methyl-thiophene metalation.



Next, the kinetic isotope effect (KIE) of deuteration at the C5-position of 2-methyl-thiophene was measured in independent reactions under catalytic conditions. A  $k_{\text{H}}/k_{\text{D}}$  of 1.2 for the C–H zincation of 2-methyl-thiophene was determined. This low value indicates that C–H bond cleavage is not involved in the turnover-limiting step of C–H zincation.

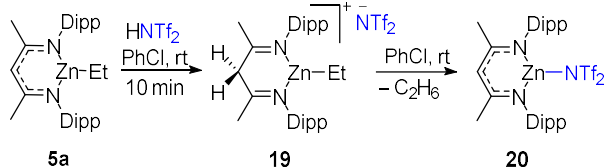
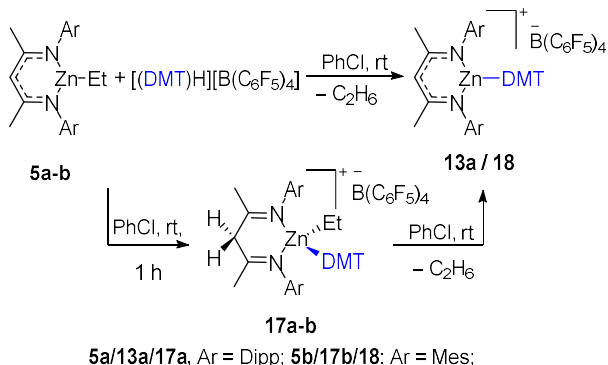
Notably, during the catalytic C–H zincation of 5-d-2-methyl-thiophene,  $^1\text{H}$  and  $^2\text{H}$  NMR spectra revealed deuterium incorporation into the  $\text{C}_\gamma$  position of the  $\text{NacNac}$  ligand (Fig. S162). The protonation of the  $\text{C}_\gamma$  position of  $\text{NacNacZnH}$  by  $[(\text{Et}_3\text{N})\text{D}]^+$  (formed by deprotonation of 5-d-2-methyl-thiophene during C–D zincation) to form a species such as **16** (Scheme 5) would account for deuterium incorporation. While there is precedence for the  $\text{C}_\gamma$  protonation of  $\text{NacNacM}$  complexes,<sup>29</sup> including a limited number of examples where the Brønsted acid is an ammonium salt,<sup>30</sup> it is unprecedented to our knowledge that protonation of the  $\text{NacNac}$  backbone proceeds in preference to protonation of a  $\text{M-H}$  unit. Although we note, as intermediates are often not observed, without labelling studies this could have been overlooked previously.

**Scheme 5.** Top, the KIE for C–H zincation of 2-methyl-thiophene. Bottom, proposed protonation of the C $\gamma$  position.



As noted earlier, no intermediates were observed during any of the dehydrocoupling reactions between ammonium cations and  $\text{NaCNacZnH}$  or between  $\text{NaCNacZnEt}$  and  $[(\text{Et}_3\text{N})\text{H}]^+$ . However, on investigating the stoichiometric reaction of  $\text{NaCNacZnEt}$  complexes **5a/b** with the more acidic ammonium salt  $[(\text{DMT})\text{H}][\text{B}(\text{C}_6\text{F}_5)_4]$  at room temperature *in-situ* NMR spectra revealed the presence of an intermediate. This intermediate slowly converted to **13a/18** and ethane (Scheme 6). In these cases, the protonation of the  $\text{NaCNac}$  backbone to form **17a** and **17b** is proposed, but analysis of these reactions revealed a substantially broadened  $\gamma\text{-CH}_2$  resonance in the  $^1\text{H}$  NMR spectra even at low temperature (in  $\text{PhCl}$ , Fig. S168), precluding definitive characterization of backbone protonation and formation of **17a/b**.

**Scheme 6.** Proposed  $\text{NaCNac}$  backbone protonation by  $[(\text{DMT})\text{H}][\text{B}(\text{C}_6\text{F}_5)_4]$  (top) and observed protonation by  $\text{HNTf}_2$  (bottom).



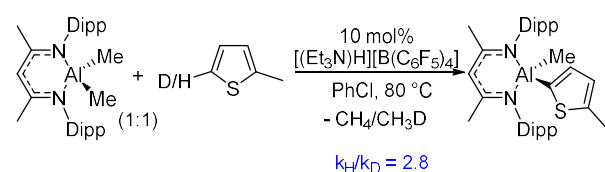
Seeking definitive evidence for backbone protonation, the reaction of  $\text{NaCNacZnEt}$  with the strong Brønsted acid  $\text{HNTf}_2$  was investigated. This produced a new compound with a singlet at  $\delta$  4.29 in  $^1\text{H}$  NMR spectrum, integrating to 2H and assigned to backbone C $\gamma$  methylene protons (Fig. S174). This is consistent with the formation of compound **19**, a conclusion supported by the  $^{13}\text{C}\{^1\text{H}\}$  NMR spectrum containing a resonance for a methylene ( $\gamma$ ) carbon at  $\delta$  45.6.<sup>31</sup> A

resonance at  $\delta -77.9$  in the  $^{19}\text{F}$  NMR spectrum of **19** indicated a non-coordinated  $\text{NTf}_2$  anion. Combined, this resulted in the formulation of **19** as a three-coordinate zinc complex, consistent with the observed solution symmetry for the NacNac ligand. Compound **19** converted into compound **20** at room temperature over time by loss of ethane. Compound **20** has a 1H integral resonance for the  $\gamma$ -CH at  $\delta 4.91$  in the  $^1\text{H}$  NMR spectrum (the corresponding carbon resonates at  $\delta 95.6$  in the  $^{13}\text{C}\{^1\text{H}\}$  NMR spectrum). The occurrence of backbone protonation prior to dehydrocoupling with the Zn-H unit while notable does not unambiguously confirm that this is an on-cycle process. Reversible  $\text{C}_\gamma$  protonation followed by direct protonolysis of Zn-H is also feasible, therefore DFT studies were performed to investigate the mechanism further (*vide infra*).

For the C-H almination of 2-methyl-thiophene, a  $k_{\text{H}}/k_{\text{D}}$  of 2.8 was observed based on independent reactions under catalytic conditions. In contrast to the zinc system, this indicates that a C-H bond cleavage is involved in the turnover-limiting step for C-H almination. Further contrasts between the Zn/Al systems were forthcoming from analysis of the  $^1\text{H}$  and  $^2\text{H}$  NMR spectra which revealed minimal deuterium incorporation into the NacNac  $\text{C}_\gamma$  position during C-H almination even after long reaction times (Fig. S181). This suggested a mechanistic divergence in these C-H zincation and C-H almination reactions.

Finally, to help benchmark the computational studies (*vide infra*) an Eyring analysis was performed for the irreversible reaction between  $\text{NacNacAlMe}_2$  (**8**) and  $[(\text{Et}_3\text{N})\text{H}][\text{B}(\text{C}_6\text{F}_5)_4]$  which forms **15b** and methane (Fig. S183). This led to a  $\Delta G^\ddagger = 21.1 (\pm 1)$  kcal/mol for this step (at 298 K).

**Scheme 7.** Determination of C-H almination KIE.



## Computational Studies on the Mechanism of C–H Zincation and C–H Alumination

The catalytic C–H metalation reactions were modelled with 2-methyl-thiophene, **2a**, as a prototypical substrate using the full NacNac ligand. Geometry optimizations employed the BP86 functional and a modest basis set (Zn: SDD; Al/S: SDD with polarization; other atoms: 6-31G\*\*). Electronic energies were then corrected for the effects of solvation (PhCl, PCM) and dispersion (DFT-D3(BJ)) and recomputed with the def2-TZVP basis set using the B3PW91 functional. The thermochemical corrections from the BP86 frequency calculations were then added to give the free energies quoted in the text. This protocol was selected after extensive functional testing and conformational searching of key stationary points involving a bound  $\text{NEt}_3$  ligand (Tables S6 and S7).

The computed profile for the catalytic zincation of **2a** is shown in Figure 4(a), where  $[\text{NacNacZn}(\text{NEt}_3)]^+$  (**13c<sup>+</sup>**) is taken as the starting point of the cycle. Overall, the reaction proceeds as postulated, with an endergonic C–H zincation to form  $\text{NacNacZn}(\text{thiophenyl})$  **3a** and  $[(\text{Et}_3\text{N})\text{H}]^+$  ( $\Delta G = +7.7$  kcal/mol) being driven forward by exergonic dehydrocoupling with  $\text{NacNacZnH}$ , **1**, to reform **13c<sup>+</sup>** with loss of  $\text{H}_2$  ( $\Delta G = -8.9$  kcal/mol). The overall process is therefore exergonic ( $\Delta G = -1.2$  kcal/mol). The mechanism of C–H zincation initiates with the associative substitution of  $\text{NEt}_3$  in **13c<sup>+</sup>** by 2-methyl-thiophene via **TS1<sup>CHZn</sup>** at +25.9 kcal/mol to form **Int1<sup>CHZn</sup>** at +11.6 kcal/mol. **Int1<sup>CHZn</sup>** shows elongation of the C<sub>4</sub>–C<sub>5</sub> thiophene bond (1.43 Å cf. 1.38 Å in free 2-methyl-thiophene), consistent with the electrophilic activation of the substrate. Deprotonation by the now free  $\text{NEt}_3$  base proceeds via **TS2<sup>CHZn</sup>** (+24.8 kcal/mol) to give **3a** and  $[(\text{Et}_3\text{N})\text{H}]^+$  at +7.7 kcal/mol. Two mechanisms were then characterized for the dehydrocoupling between **1** and  $[(\text{Et}_3\text{N})\text{H}]^+$ : (i) direct protonolysis of the Zn–H bond, and (ii) a ligand-assisted process. Of these, the latter proved significantly more accessible and proceeds through protonation of the  $\gamma$ -C position of the NacNac backbone via **TS1<sup>DHCZn</sup>** at +19.7 kcal/mol to give initially a H-bonded adduct (not shown) from which  $\text{NEt}_3$  dissociation forms **Int1<sup>DHCZn</sup>**.  $\text{NEt}_3$  coordination at Zn then gives **Int2<sup>DHCZn</sup>** at +16.3 kcal/mol. The  $\text{ZnN}_2\text{C}_3$  metallacycle in **Int2<sup>DHCZn</sup>** (Figure 4b, bottom) exhibits a boat structure with a relatively short C–H $\cdots$ H–Zn contact of 2.23 Å.  $\text{H}_2$  loss then proceeds with a barrier of only 9.2 kcal/mol via **TS3<sup>DHCZn</sup>** at +25.5 kcal/mol, that exhibits elongated C–H and Zn–H distances (1.44 Å and 1.79 Å respectively) and incipient H–H bond formation (C–H $\cdots$ H–Zn = 1.00 Å). The alternative direct protonolysis of the Zn–H bond in **1** entails a larger barrier of 25.4 kcal/mol via **TS4<sup>DHCZn</sup>** at +33.1 kcal/mol (depicted in grey, Figure 4(a) and Figure 4(b) top).

The reaction profile for the C–H zincation of **2a** was next computed with DMT for which the ligand-assisted dehydrocoupling pathway again has a lower overall barrier (Fig. S188). Comparing the free energy spans shows  $\text{NEt}_3$  should be better for catalysis compared to DMT,  $\Delta G^\ddagger_{\text{span}} = 25.9$  vs. +27.4 kcal/mol, consistent with the experimental results. Again, the overall barrier is dominated by two factors: (i) how endergonic the C–H metalation phase is, and (ii) the magnitude of the dehydrocoupling barrier. With DMT, dehydrocoupling has a lower overall barrier (11.9 kcal/mol) relative to  $\text{Et}_3\text{N}$  (17.8 kcal/mol) consistent with the relative reactivity of **1** and the respective  $[(\text{R}_3\text{N})\text{H}]^+$  salts. The lower dehydrocoupling barrier with DMT originates from the  $\gamma$ -C protonation of **1** being effectively energetically neutral with  $[(\text{DMT})\text{H}]^+$  (-0.1 kcal/mol to form the DMT analogue of **Int2<sup>DHCZn</sup>**), in contrast to being uphill using the less acidic  $[(\text{Et}_3\text{N})\text{H}]^+$ . However, C–H zincation is significantly more endergonic with DMT (+15.5 kcal/mol to form **3a**), and this results in the overall higher  $\Delta G^\ddagger_{\text{span}}$  for DMT vs  $\text{Et}_3\text{N}$ .

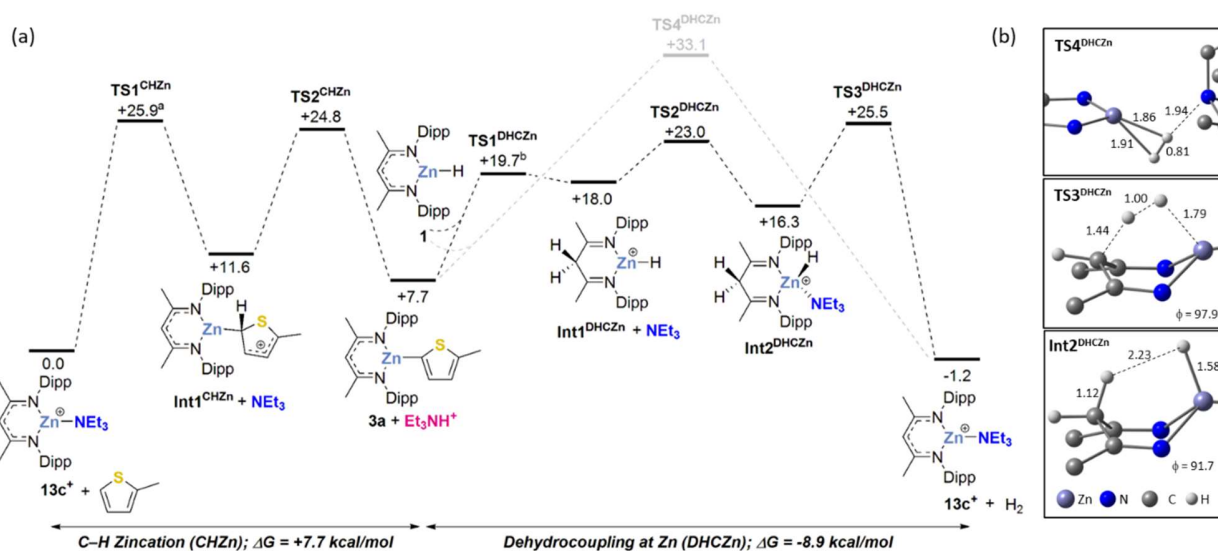


**Figure 4.** (a) Computed free energy reaction profile (kcal/mol) for the catalytic C–H zincation of 2-methyl-thiophene (Method: B3PW91(def2-TZVP, D3(BJ), PhCl)//BP86(Zn: SDD; S: SDD(d); other atoms: 6-31G\*\*). <sup>a</sup> a precursor complex was located at +13.2 kcal/mol; <sup>b</sup> **TS1**<sup>DHCZn</sup> leads initially to a H-bonded NEt<sub>3</sub> adduct at +17.9 kcal/mol that is omitted for brevity (see supporting materials). (b) Details of selected stationary points (distances in Å; φ = metallacycle folding angle, see text for details; NacNac Dipp groups, Me H atoms and NEt<sub>3</sub> H atoms omitted for clarity).

The computed profile for the C–H alumination of **2a** is shown in Figure 5(a). Starting from the 4-coordinate cationic NEt<sub>3</sub> adduct [NacNacAl(Me)(NEt<sub>3</sub>)]<sup>+</sup>, **15b**<sup>+</sup>, the reaction proceeds via the dissociative substitution of NEt<sub>3</sub> by **2a** to form the electrophilically activated adduct **Int2**<sup>CHAl</sup> at +6.8 kcal/mol. Deprotonation of this species by free NEt<sub>3</sub> then gives **9a**, plus [(Et<sub>3</sub>N)H]<sup>+</sup> at +4.2 kcal/mol. This endergonic C–H alumination is followed by an exergonic dehydrocoupling between **8** and [(Et<sub>3</sub>N)H]<sup>+</sup> to reform **15b**<sup>+</sup> along with CH<sub>4</sub> (ΔG = -15.1 kcal/mol). The overall catalytic cycle is therefore exergonic (ΔG = -10.9 kcal/mol). Calculation of the ligand-assisted protonolysis pathway for Al revealed that while protonation at the NacNac γ-C is kinetically accessible via **TS2**<sup>DHCAI</sup> at +19.4 kcal/mol, the subsequent CH<sub>4</sub> elimination via **TS3**<sup>DHCAI</sup> is much higher at +36.1 kcal/mol. However, in this case direct protonolysis is more accessible via **TS1**<sup>DHCAI</sup> (at +24.9 kcal/mol), with this corresponding to a Me-abstraction involving a near-linear Al⋯CH<sub>3</sub>⋯H⋯NEt<sub>3</sub> unit (Figure 4(b) top). Binding of Et<sub>3</sub>N to Al then occurs in a separate step to reform **15b**<sup>+</sup>. It is noteworthy that protonolysis (methane loss) and amine binding occur in separate steps in this pathway due to the accessibility of the amine-free cation, [NacNacAl–Me]<sup>+</sup> (note, this cation has been previously reported).<sup>27</sup> In contrast, in the zinc system forming the amine-free cation, [NacNacZn]<sup>+</sup>, results in high energy intermediates (>30 kcal/mol, see Fig. S187), precluding a comparable pathway involving direct Zn–H protonolysis followed by a separate amine binding step.

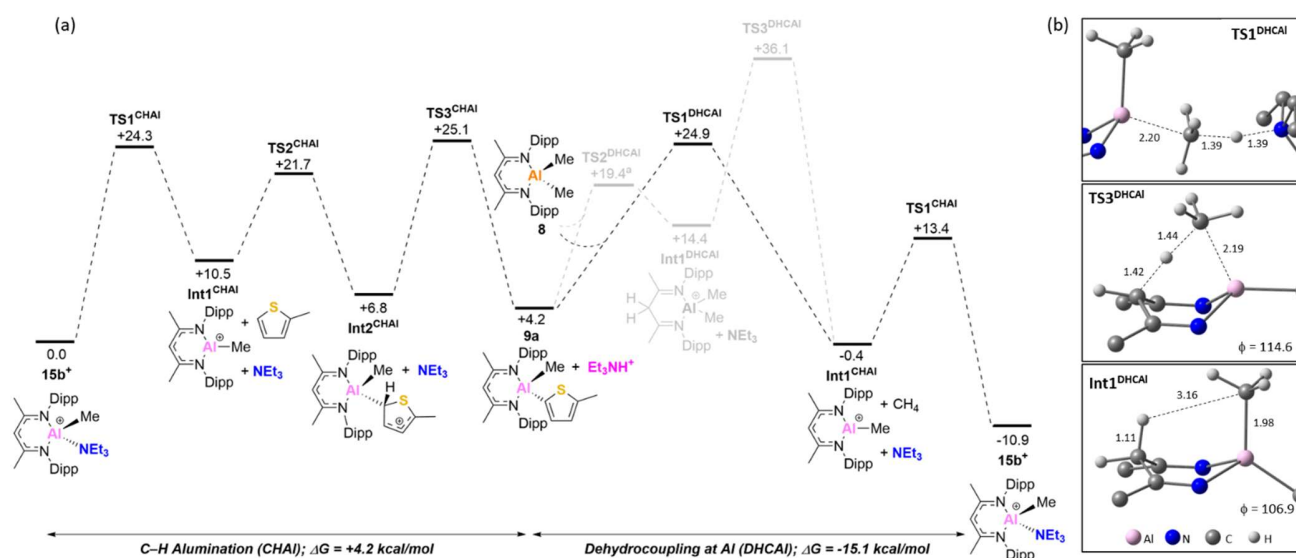


**Figure 5.** (a) Computed free energy reaction profile (kcal/mol) for the catalytic C–H aluminations of 2-methylthiophene (Method: B3PW91(def2-TZVP, D3(BJ), PhCl)/BP86(Al/S: SDD(d); other atoms: 6-31G\*\*). <sup>a</sup> **TS2**<sup>DHCAI</sup> leads initially to a H-bonded NEt<sub>3</sub> adduct at +17.5 kcal/mol that is omitted for brevity (see supporting materials for details). (b) Details of selected stationary points (distances in Å;  $\phi$  = metallacycle folding angle, see text for details; NacNac Dipp groups, Me H atoms and NEt<sub>3</sub> H atoms omitted for clarity).

The computed reaction profiles in Figures 4 and 5 capture many of the key reactivity patterns seen experimentally. Both C–H zincation and aluminations reactions are endergonic and the metalated products are trapped through exergonic dehydrocoupling. The computed barrier for the protonolysis of **1** to form **13c**<sup>+</sup> (17.8 kcal/mol) is lower than that for **8** to form **15b**<sup>+</sup> (20.7 kcal/mol), consistent with the relative solution reactivities. Furthermore, the computed barrier for the dehydrocoupling of **8** with [(Et<sub>3</sub>N)H]<sup>+</sup> (20.7 kcal/mol) is in good agreement with the experimental value of 21.1 (±1) kcal/mol, and this barrier is lower than that for the protonolysis of **9a**, albeit only by 0.2 kcal/mol. The last comparison is clearly subtle, and this extends to the interpretation of the experimental *k*<sub>H</sub>/*k*<sub>D</sub> KIEs. Thus, the low KIE of 1.2 for the catalytic zincation of **2a** (Scheme 5) is consistent with the computed rate-limiting transition state, **TS1**<sup>CHZn</sup>, that corresponds to associative NEt<sub>3</sub>/**2a** substitution. In contrast, **TS3**<sup>CHAI</sup> is computed to be rate-limiting for catalytic aluminations and this does involve C–H bond cleavage, aligning with the larger KIE of 2.8 (Scheme 7). More generally, however, both cycles involve several high energy transition states of varying character that are close in energy, and for which the relative energetic ordering is functional dependent. The B3PW91 functional was chosen as it performs qualitatively the best over the range of available experimental mechanistic data; a more quantitative interpretation of the computed profiles would be challenging.

While both the C–H zincation and aluminations reactions follow the same general pattern of sequential C–H activation/dehydrocoupling, these two processes do differ in the details. In some cases, this reflects the valency of the metal centers; NEt<sub>3</sub>/**2a** substitution is an associative substitution at the 3-coordinate Zn in **13c**<sup>+</sup>, whereas starting from the 4-coordinate Al complex **15b**<sup>+</sup> substitution proceeds via a dissociative process. Furthermore, direct protonolysis of the Zn–H bond in **1** involves approach of [(Et<sub>3</sub>N)H]<sup>+</sup> from above the coordination plane in **TS4**<sup>DHCZn</sup>, with concerted Zn–H bond cleavage and Zn–NEt<sub>3</sub> bond formation necessary to avoid the intermediacy of the high energy two coordinate [NacNacZn]<sup>+</sup> cation. In contrast, such an approach is not found for the direct protonolysis of the Al–Me bond

in **8** and instead [(Et<sub>3</sub>N)H]<sup>+</sup> engages in an essentially linear Me abstraction via **TS1<sup>DHCAI</sup>**. This is presumably due to the higher coordination number (four in **8** vs. three in **1**) and the fact that the amine-free cation [NacNacAl–Me]<sup>+</sup> is energetically accessible.<sup>26, 27</sup>

Notably, the barrier to ligand-assisted H<sub>2</sub> loss from **Int2<sup>DHCzn</sup>** ( $\Delta G^\ddagger = 9.2$  kcal/mol) is much lower than that for ligand-assisted CH<sub>4</sub> loss from **Int1<sup>DHCAI</sup>** ( $\Delta G^\ddagger = 21.7$  kcal/mol). This significant difference combined with the ubiquity of NacNacM complexes in chemistry<sup>32</sup> means the factors impacting the barrier to dehydrocoupling via the ligand assisted pathway warrant further discussion. Two main factors appear to underpin this barrier:

(i) H atom transfer is facilitated by the isotropic H 1s orbital that facilitates overlap in the transition state, whereas Me group transfer involves distortion of the more directional sp<sup>3</sup> hybrid (as indicated by NBO analyses on these two systems, Figure 6 and S197).<sup>33</sup> This difference may be enhanced to some extent by the dominant Zn 4s character in the Zn–H bond in **Int3<sup>DHCzn</sup>**; in contrast the Al contribution to the Al–Me bond in **Int1<sup>DHCAI</sup>** has more directional sp<sup>1.2</sup> character (consistent with the relative energy of the 4s vs. 4p orbitals for zinc and the 3s vs. 3p orbitals for aluminum, with the Zn 4p orbitals being relatively high in energy).<sup>20</sup> The residual Al⋯Me interaction is further undermined in **TS3<sup>DHCAI</sup>** compared to the Zn⋯H interaction in **TS3<sup>DHCzn</sup>**.

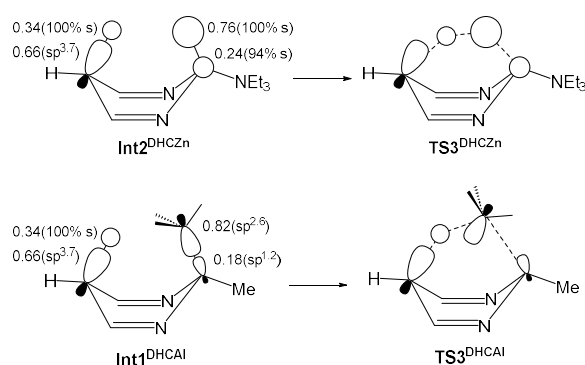


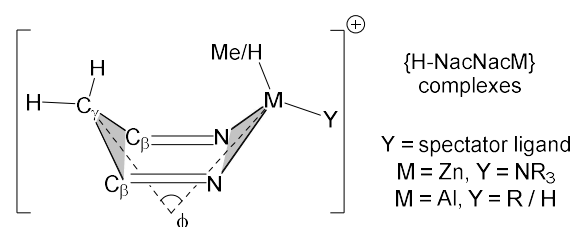
**Figure 6.** Coefficients and hybridization of the  $\sigma_{\text{Zn-H}}$  NBO in **Int2<sup>DHCzn</sup>**, the  $\sigma_{\text{Al-Me}}$  NBO in **Int1<sup>DHCAI</sup>** and the  $\sigma_{\text{C-H}}$  NBOs. The impact on orbital overlap in the corresponding transition states is shown schematically (see also Figure S197).

(ii) the degree of pre-organization into a boat-like conformation in the precursor complexes, quantified by  $\phi$ , the metallacycle folding angle between the NMN (M = Zn, Al) and C<sub>γ</sub>C<sub>β</sub>C<sub>β</sub> planes that define the ‘bow’ and ‘stern’ of the boat. In **Int2<sup>DHCzn</sup>**  $\phi = 91.7^\circ$ , resulting in a short H⋯H contact of 2.23 Å, and this distortion decreases ( $\phi$  increases to 97.9°) in **TS3<sup>DHCzn</sup>**. In contrast, **Int1<sup>DHCAI</sup>** has  $\phi = 114.6^\circ$  (C⋯H = 3.16 Å) and the distortion increases to access **TS3<sup>DHCAI</sup>** ( $\phi = 106.9^\circ$ ). Notably, larger spectator ligands (defined as Y, Table 5) at the metal promote the ligand-assisted H<sub>2</sub> or CH<sub>4</sub> loss reactions by increasing the distortion (decreasing  $\phi$ ) of the precursor complexes (*vide infra*).

These factors were explored further by computing the ligand-assisted dehydrocoupling step in a series of model complexes (Table 5). [H–NacNacZnH(NEt<sub>3</sub>)]<sup>+</sup> (i.e. **Int3<sup>DHCzn</sup>**) and the Me-analogue, [H–NacNacZnMe(NEt<sub>3</sub>)]<sup>+</sup> (Entry 1 vs. 2), show similar  $\phi$  values, and the higher barrier to CH<sub>4</sub> loss is consistent with the detrimental directionality effect associated with alkyl transfer. This is fully consistent with C–H zincation using NacNacZn–Et not being successful due to the larger  $\Delta G^\ddagger_{\text{span}}$  produced by this effect (see Fig. S190). Similarly, CH<sub>4</sub> loss from [H–NacNacAlMe<sub>2</sub>]<sup>+</sup> (**Int1<sup>DHCAI</sup>**) is

harder than H<sub>2</sub> loss from the corresponding dihydride [H–NacNacAlH<sub>2</sub>]<sup>+</sup> (Entry 3 vs. 4). However, this comparison is complicated by large differences in  $\phi$ , with [H–NacNacAlMe<sub>2</sub>]<sup>+</sup> showing a much greater distortion to a boat conformation ( $\phi = 114.6^\circ$  cf.  $145.7^\circ$ ). The isomers of the mixed H/Me species confirm the spectator ligand effect: [H–NacNacAl(H)Me]<sup>+</sup> (Me spectator) shows a large distortion ( $\phi = 113.5^\circ$ ) that lowers the barrier to H<sub>2</sub> loss compared to [H–NacNacAlH<sub>2</sub>]<sup>+</sup> (Entry 4 vs. 5); the alternative [H–NacNacAl(Me)H]<sup>+</sup> isomer (H spectator) shows a low distortion ( $\phi = 139.0^\circ$ ) and CH<sub>4</sub> loss is harder than [H–NacNacAlMe<sub>2</sub>]<sup>+</sup> (entry 3 vs. 6). Introducing a bulkier <sup>t</sup>Bu spectator group (Entry 7) reiterates this effect, increasing the distortion ( $\phi = 102.7^\circ$ ) and reducing the barrier to H<sub>2</sub> loss even further to 11.3 kcal/mol (See Fig S194).

**Table 5.** Computed barriers (kcal/mol) for loss of H<sub>2</sub>/MeH from the direct precursor (e.g., **Int2**<sup>DHCZn</sup> or **Int1**<sup>DHAl</sup>) and geometric distortions (quantified by the interplane angle  $\phi$ ), in model Zn and Al complexes. Values of  $\phi$  are for precursor/transition state.



	Precursor Complex	$\Delta G^\ddagger$	$\phi$ (°)
1	[H–NacNacZnH(NEt <sub>3</sub> )] <sup>+</sup>	9.2	91.7/97.9
2	[H–NacNacZnMe(NEt <sub>3</sub> )] <sup>+</sup>	16.0	92.8/90.3
3	[H–NacNacAlMe <sub>2</sub> ] <sup>+</sup>	21.7	114.6/106.9
4	[H–NacNacAlH <sub>2</sub> ] <sup>+</sup>	16.7	145.7/105.0
5	[H–NacNacAl(H)Me] <sup>+</sup>	14.1	113.5/104.7
6	[H–NacNacAl(Me)H] <sup>+</sup>	25.1	139.0/96.3
7	[H–NacNacAl(H) <sup>t</sup> Bu] <sup>+</sup>	11.3	102.7/104.2
8	[H–NacNacZnH(NMe <sub>3</sub> )] <sup>+</sup>	11.4	94.2/99.2
9	[H–NacNacZnH(NH <sub>3</sub> )] <sup>+</sup>	13.9	106.6/100.3

A related effect is observed in the zinc system on varying the amine spectator ligand: replacing NEt<sub>3</sub> with smaller amines (NMe<sub>3</sub> and NH<sub>3</sub>, compare Entries 8 and 9 to Entry 1) decreases the distortion in the precursor (higher  $\phi$ ) and leads to higher barriers to H<sub>2</sub> loss.<sup>34</sup> It is also notable that the closest Al/Zn pairs, in terms of steric demand of the spectator ligand (entries 7 and 8 and entries 5 and 9), have extremely similar barriers to H<sub>2</sub> loss (11.3 vs. 11.4 and 14.1 vs. 13.9 kcal/mol), indicating that in these systems the steric bulk of the spectator ligand plays a greater role in determining the barrier to dehydrocoupling than the identity of the metal and the nature of the M–Y interaction. It is notable that the kinetically most accessible dehydrocoupling reactions (Entries 1 and 7) involve H<sub>2</sub> loss in the presence of the bulkiest spectator ligand explored; the latter pre-organizes the system to such an extent that  $\phi$  actually increases (i.e., the

distortion decreases) in the transition state. This significant effect (up to 5 kcal/mol  $\delta\Delta G^\ddagger$  in the series studied herein) has implications for the design of NacNacM catalysts, as it suggests that increasing the steric bulk around the metal center can actually be desirable for lower barrier protonolysis processes via a ligand-assisted mechanism.

## Conclusions

By coupling an endergonic C–H metalation step with a subsequent exergonic dehydrocoupling step we have developed the first catalytic transition metal-free heteroarene C–H zincation/ C–H alumination requiring only sub-stoichiometric base. This process uses readily accessible NacNacM complexes and simple amines, such as Et<sub>3</sub>N, as the base.

The properties of the base are crucial for an effective process since it fulfils multiple roles: coordination to M and deprotonation of the [M-(heteroaryl-H)]<sup>+</sup> complex, with the resultant [(Base)H]<sup>+</sup> then key for protonating the Zn–H/Al–Me containing complex. Initial guidelines for selecting an appropriate base include: (i) sufficiently low nucleophilicity towards M to enable displacement by an incoming heteroarene; (ii) sufficient basicity to deprotonate the resultant [M-(heteroaryl-H)]<sup>+</sup> complex. Furthermore, combining (i) and (ii) needs to produce a C–H metalation phase that is not too uphill energetically. This is crucial as a significantly endergonic metalation phase will increase the overall energy span of the process once the barrier in the second half of the catalytic cycle, the dehydrocoupling phase, is taken into account, potentially making it too high to proceed. Given that C–H metalation is endergonic, the dehydrocoupling step needs to have a relatively low barrier pathway for the overall cycle to be energetically feasible.

Notably, with NacNac ligands there is a degree of mechanistic flexibility in the dehydrocoupling step due to the possibility of direct protonation of the M–H/M–Me unit or ligand non-innocence (backbone protonation) mediating subsequent dehydrocoupling. Computational analysis of both pathways revealed the lowest energy route is predominantly dictated by (i) the accessibility of the amine-free [NacNacM]<sup>+</sup> complex and (ii) the degree of steric-derived distortion towards a boat conformer upon backbone protonation. For example, with the aluminum system an amine-free cation ([NacNacAlMe]<sup>+</sup>) is energetically accessible enabling protonolysis to proceed in a separate step to Al-amine bond formation. However, for the zinc system no amine-free cation ([NacNacZn]<sup>+</sup>) is energetically accessible, precluding a stepwise Zn–H protonation-amine binding process, resulting in an alternative mechanism that proceeds via ligand non-innocence. With other ligands backbone protonation may not be feasible therefore careful selection of the organometallic complex is essential to avoid high energy intermediates/barriers during dehydrocoupling that would therefore preclude catalytic C–H metalation. Based on the insights afforded from this initial study, and the fact it is applicable to two disparate metals (Zn and Al) we believe that multiple other main group metals and other ligand sets will be amenable to this transition metal-free, catalytic in base, C–H metalation approach. Thus, it has the potential to facilitate the synthesis of a range of important organometallic reagents.

## ASSOCIATED CONTENT

### Data Availability Statement

The data underlying this study are available in the published article and its Supporting Information.

### Accession Codes

CCDC 2330581-2330586 and 2330578 contain the supplementary crystallographic data for this paper. These data can be obtained free of charge via [www.ccdc.cam.ac.uk/data\\_request/cif](http://www.ccdc.cam.ac.uk/data_request/cif), or by emailing [data\\_request@ccdc.cam.ac.uk](mailto:data_request@ccdc.cam.ac.uk), or by contacting The Cambridge Crystallographic Data Centre, 12 Union Road, Cambridge CB2 1EZ, UK; fax: +441223336033.

## **AUTHOR INFORMATION**

### **Corresponding Author**

\*[michael.ingleson@ed.ac.uk](mailto:michael.ingleson@ed.ac.uk)

\*[sam38@st-andrews.ac.uk](mailto:sam38@st-andrews.ac.uk)

### **Author Contributions**

‡ = these two authors contributed equally to the manuscript. MKB performed all the experimental work in this manuscript and JL performed the vast majority of the computational work. GSN collected and solved all the X-ray structures. The manuscript was written through the contributions of all authors. All authors have given approval to the final version of the manuscript.

### **Funding Sources**

The EPSRC, (EP/V03829X and EP/T019867/1).

The University of Edinburgh

## **ACKNOWLEDGMENTS**

This project has received funding from the European Research Council under the European Union's Horizon 2020 research and innovation program (grant agreement No 769599), the University of Edinburgh and the EPSRC (EP/V03829X and EP/T019867/1). We thank the Mass Spectrometry facility (SIRCAMS) at the University of Edinburgh (UoE) for carrying out MS analysis. We also acknowledge Prof. Guy Lloyd-Jones and Dr Dominic Willcox for useful discussions.

## REFERENCES

- (1) For select reviews on C–H functionalization see: (a) Docherty, J. H.; Lister, T. M.; McArthur, G.; Findlay, M. T.; Domingo-Legarda, P.; Kenyon, J.; Choudhary, S.; Larrosa, I.; Transition-Metal-Catalyzed C–H Bond Activation for the Formation of C–C Bonds in Complex Molecules. *Chem. Rev.* **2023**, *123*, 7692–7760. (b) Dalton, T.; Faber, T.; Glorius, F.; C–H Activation: Toward Sustainability and Applications, *ACS Cent. Sci.* **2021**, *7*, 245–261.
- (2) For recent reviews on metal-catalyzed C–H borylation see: (a) Guria, S.; Hassan, M. M. M.; Chattopadhyay, B.; C–H borylation: a tool for molecular diversification, *Org. Chem. Front.* **2024**, Advance Article <https://doi.org/10.1039/D3Q001931D>. (b) Bisht, R.; Haldar, C.; Hassan, M. M. M.; Hoque, M. E.; Chaturvedi, J.; Chattopadhyay, B.; Metal-catalysed C–H bond activation and borylation. *Chem. Soc. Rev.* **2022**, *51*, 5042–5100.
- (3) For a recent review on C–H silylation see: Khatua, H.; Das, S.; Patra, S.; Chattopadhyay, B.; C–H Bond Silylation of Heteroarenes, *Synthesis* **2023**, *55*, 3434–3453.
- (4) For recent reviews covering this topic see: (a) Judge, N. R.; Logallo, A.; Hevia, E.; Main group metal-mediated strategies for C–H and C–F bond activation and functionalisation of fluoroarenes. *Chem. Sci.* **2023**, *14*, 11617–11628. (b) Batuecas, M.; Gorgas, N.; Crimmin, M. R.; Catalytic C–H to C–M (M = Al, Mg) bond transformations with heterometallic complexes. *Chem. Sci.* **2021**, *12*, 1993–2000.
- (5) For select papers on the utility of organoaluminum reagents see: (a) Knochel, P.; Blümke, T.; Groll, K.; Chen, Y.-H.; Preparation of Organoalanes for Organic Synthesis, *Top. Organomet. Chem.* **2013**, *41*, 173–186. (b) Ogawa, H.; Yang, Z. K.; Minami, H.; Kojima, K.; Saito, T.; Wang, C.; Uchiyama, M.; Revisitation of Organoaluminum Reagents Affords a Versatile Protocol for C–X (X = N, O, F) Bond-Cleavage Cross-Coupling: A Systematic Study. *ACS Catal.* **2017**, *7*, 3988–3994. (c) Minami, H.; Saito, T.; Wang, C.; Uchiyama, M.; Organoaluminum-Mediated Direct Cross-Coupling Reactions. *Angew. Chem. Int. Ed.*, **2015**, *54*, 4665–4668.
- (6) For reviews on the utilization of organozinc reagents see: (a) Wei, B.; Knochel, P.; Recent Advances in Cross-Couplings of Functionalized Organozinc Reagents. *Synthesis* **2022**, *54*, 246–254. (b) Dilmann, A. D.; Levin, V. V.; Advances in the chemistry of organozinc reagents, *Tet. Lett.* **2016**, *57*, 3986–3992.
- (7) ICH guideline Q3D (R2) on elemental impurities see: [https://www.ema.europa.eu/en/documents/scientific-guideline/international-conference-harmonisation-technical-requirements-registration-pharmaceuticals-human-use-ich-q3d-elemental-impurities-step-5-revision-2\\_en.pdf](https://www.ema.europa.eu/en/documents/scientific-guideline/international-conference-harmonisation-technical-requirements-registration-pharmaceuticals-human-use-ich-q3d-elemental-impurities-step-5-revision-2_en.pdf) (accessed 26/1/2024). Note, for Al and Zn permitted daily exposure limits have not been defined due to their low toxicity.
- (8) For representative example of C–H zincation stoichiometric in strong base (a) Generation of Functionalized Asymmetric Benzynes with TMP-Zincates. Effects of Ligands on Selectivity and Reactivity of Zincates. Uchiyama, M.; Miyoshi, T.; Kajihara, Y.; Sakamoto, T.; Otani, Y.; Ohwada, T.; Kondo, Y.; *J. Am. Chem. Soc.* **2002**, *124*, 8514–8515; (b) Wunderlich, S.; Knochel, P.; (tmp)<sub>2</sub>Zn<sub>2</sub>MgCl<sub>2</sub>·2 LiCl: A Chemoselective Base for the Directed Zincation of Sensitive Arenes and Heteroarenes. *Angew. Chem., Int. Ed.* **2007**, *46*, 7685–7688; (c) Mastropierro, P.; Kennedy, A. R.; Hevia, E.; Metallation of sensitive fluoroarenes using a potassium TMP-zincate supported by a silyl(bis)amido ligand. *Chem. Commun.* **2022**, *58*, 5292–5295. (d) Judge, N.; Hevia, E.; Alkali-Metal-Alkoxide Powered Zincation of Fluoroarenes Employing Zinc Bis-Amide Zn(TMP)<sub>2</sub>. *Angew. Chem. Int. Ed.* **2023**, *62*, e202303099.
- (9) For representative example of C–H alumination stoichiometric in strong base see: (a) Naka, H.; Uchiyama, M.; Matsumoto, Y.; Wheatley, A. E. H.; McPartlin, M.; Morey, J. V.; Kondo, Y.; An Aluminum Ate Base: Its Design, Structure, Function, and Reaction Mechanism. *J. Am. Chem. Soc.* **2007**, *129*, 1921–1930. (b) Wunderlich, S. H.; Knochel, P.

Aluminum Bases for the Highly Chemoselective Preparation of Aryl and Heteroaryl Aluminum Compounds. *Angew. Chem. Int. Ed.* **2009**, *48*, 1501–1504. (c) McLellan, R.; Uzelac, M.; Kennedy, A. R.; Hevia, E.; Mulvey, R. E.; LiTMP Trans-Metal-Trapping of Fluorinated Aromatic Molecules: A Comparative Study of Aluminum and Gallium Carbanion Traps. *Angew. Chem. Int. Ed.* **2017**, *56*, 9566–9570. Note direct arene C-H alumination has also been reported using Al(I) compounds, for example see: Hicks, J.; Vasko, P.; Goicoechea, J. M.; Aldridge, S.; Synthesis, structure and reaction chemistry of a nucleophilic aluminyl anion. *Nature* **2018**, *557*, 92–95

(10) Garçon, M.; Mun, N. W.; White, A. J. P.; Crimmin, M. R.; Palladium-Catalysed C–H Bond Zincation of Arenes: Scope, Mechanism, and the Role of Heterometallic Intermediates. *Angew. Chem. Int. Ed.* **2021**, *60*, 6145–6153.

(11) (a) Chen, W.; Hooper, T. N.; Ng, J.; White, A. J. P.; Crimmin, M. R.; Palladium-Catalyzed Carbon–Fluorine and Carbon–Hydrogen Bond Aluminations of Fluoroarenes and Heteroarenes. *Angew. Chem. Int. Ed.*, **2017**, *56*, 12687–12691. (b) Hooper, T. N.; Garçon, M.; White, A. J. P.; Crimmin, M. R.; Room temperature catalytic carbon–hydrogen bond aluminations of unactivated arenes: mechanism and selectivity. *Chem. Sci.* **2018**, *9*, 5435–5440. (c) Rekhroukh, F.; Chen, W.; Brown, R. K.; White, A. J. P.; Crimmin, M. R.; Palladium-catalysed C–F aluminations of fluorobenzenes: mechanistic diversity and origin of selectivity. *Chem. Sci.* **2020**, *11*, 7842–7849. (d) Note, very recently a vanadium catalyzed alkene C-H aluminations process has been reported, see: Vanadium Alumanyl Complex: Synthesis, Characterization, Reactivity, and Application as a Catalyst for C–H Aluminations of Alkenes. *J. Am. Chem. Soc.*, **2024**, *146*, 3492–3497.

(12) For an overview of FLP chemistry see: (a) Stephan, D. W.; Diverse Uses of the Reaction of Frustrated Lewis Pair (FLP) with Hydrogen, *J. Am. Chem. Soc.* **2021**, *137*, 10018–10032. For recent reviews on FLPs in C–H functionalization see: (b) Ingleson, M. J.; Main Group Catalyzed Arene Borylation: Challenges and Opportunities, *ACS Catal.* **2023**, *13*, 7691–7697. (c) Hazra, S.; Mahato, S.; Das, K. K.; Panda, S.; Transition-Metal-Free Heterocyclic Carbon-Boron Bond Formation. *Chem. Eur. J.* **2022**, *28*, e202200556. (d) Tan, X.; Wang, H.; Borenius-Ions in Catalytic Aromatic C–H Borylation. *ChemCatChem.* **2023**, *15*, e2023007. (e) Desrosiers, V.; Fontaine, F.-G. Boron Lewis Pair Mediated C–H activation and Borylation. *Synthesis*, **2021**, *53*, 4599–4613.

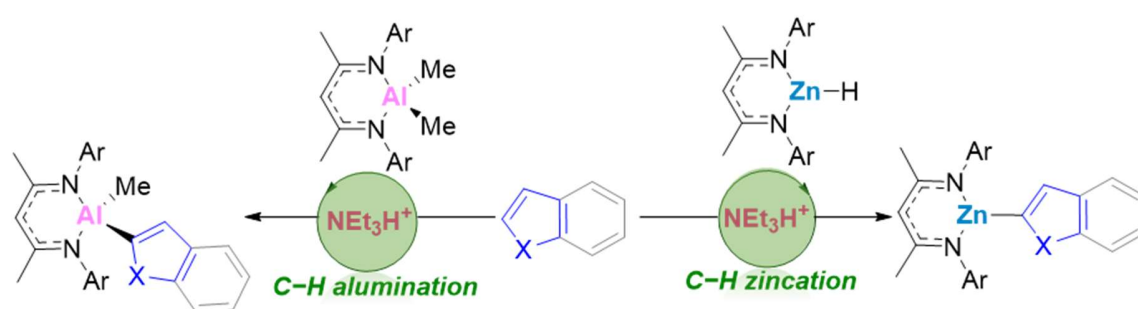
(13) For the closest borane-based example to the zinc/aluminium worked reported herein see: (a) Del Grosso, A.; Singleton, P. J.; Muryn, C. A.; Ingleson, M. J. Pinacol Boronates by Direct Arene Borylation with Borenius Cations, *Angew. Chem., Int. Ed.* **2011**, *50*, 2102–2106. (b) Yin, Q.; Klare, H. F. T.; Oestreich, M., Catalytic Friedel–Crafts C–H Borylation of Electron-Rich Arenes: Dramatic Rate Acceleration by Added Alkenes. *Angew. Chem. Int. Ed.* **2017**, *56*, 3712–3717.

(14) For Al see: (a) Stennett, T. E.; Pahl, J.; Zijlstra, H. S.; Seidel, F. W.; Harder, S.; A Frustrated Lewis Pair Based on a Cationic Aluminum Complex and Triphenylphosphine. *Organometallics* **2016**, *35*, 207–217 (b) Willcox, D. R.; De Rosa, D. M.; Howley, J.; Levy, A.; Steven, A.; Nichol, G. S.; Morrison, C. A.; Cowley, M. J.; Thomas, S. P. Aluminium-Catalyzed C(sp)–H Borylation of Alkynes. *Angew. Chem. Int. Ed.* **2021**, *60*, 20672–20677. For zinc see: (c) Grundy, M. E.; Yuan, K.; Nichol, G. S.; Ingleson, M. J.; Zinc catalysed electrophilic C–H borylation of heteroarenes. *Chem. Sci.* **2021**, *12*, 8190–8198. (d) Grundy, M. E.; Sotorrios, L.; Bisai, M. K.; Yuan, K.; Macgregor, S. A.; Ingleson, M. J. Understanding and Expanding Zinc Cation/amine Frustrated Lewis Pair Catalyzed C–H Borylation. *ACS Catal.* **2023**, *13*, 2286–2294. (e) Morris, L. J.; Rajeshkumar, T.; Okumura, A.; Maron, L.; Okuda, J.; Solvent-Dependent Oxidative Addition and Reductive Elimination of H<sub>2</sub> Across a Gallium-Zinc Bond. *Angew. Chem. Int. Ed.* **2022**, *61*, e202208855.

(15) Chen, S.; Li, B.; Wang, X.; Huang, Y.; Li, J.; Zhu, H.; Zhao, L.; Frenking, G.; Roesky, H. W. A C(sp<sup>2</sup>)–H Dehydrogenation of Heteroarene and Arenes by a Functionalized Aluminium Hydride. *Chem. Eur. J.* **2017**, *23*, 13633–13637.

- (16) Yang, Q.; Li, Y.; Yang, J.-D.; Liu, Y.; Zhang, L.; Luo, S.; Cheng, J.-P.; Holistic Prediction of pK<sub>a</sub> in Diverse Solvents Based on Machine Learning Approach, *Angew. Chem. Int. Ed.* **2020**, *59*, 19282–19291.
- (17) For Mayr's Reactivity parameters see: <https://www.cup.lmu.de/oc/mayr/reaktionsdatenbank/> (accessed on 25/01/2024).
- (18) Bagutski, V.; Del Grosso, A.; Ayuso Carrillo, J.; Cade, I. A.; Helm, M. D.; Lawson, J. R.; Singleton, P. J.; Solomon, S. A.; Marcelli, T.; Ingleson, M. J.; Mechanistic Studies into Amine-Mediated Electrophilic Arene Borylation and Its Application in MIDA Boronate Synthesis. *J. Am. Chem. Soc.* **2013**, *135*, 474–487.
- (19) (a) Desrosiers, V.; Gaudy, A.; Giroux, K.-A.; Fontaine, F.-G.; Metal-Free Transfer C–H borylation of Substituted Thiophenes. *ZAAC*, **2023**, e202300006. (b) Rochette, E.; Desrosiers, V.; Soltani, Y.; Fontaine, F.-G.; Isodesmic C–H Borylation: Perspectives and Proof of Concept of Transfer Borylation Catalysis. *J. Am. Chem. Soc.* **2019**, *141*, 12305–12311.
- (20) Rahm, M.; Zeng, T.; Hoffmann, R.; Electronegativity Seen as the Ground-State Average Valence Electron Binding Energy. *J. Am. Chem. Soc.* **2019**, *141*, 342–351.
- (21) Zhang, L.; Kaukver, S.; McMullen, J.; White, A. J. P.; Crimmin, M. R. Catalytic C–H Almination of Thiophenes: DFT Predictions and Experimental Verification. *Organometallics* **2023**, *42*, 1711–1716
- (22) This is comparable to other three coordinate [NacNacZn-L]<sup>+</sup> cations, see: Friedrich, A.; Eyselien, J.; Langer, J.; Harder, S.; Comparison of Magnesium and Zinc in Cationic  $\pi$ -Arene and Halobenzene Complexes. *Organometallics* **2021**, *40*, 448–457.
- (23) (a) Chisholm, M. H.; Gallucci, J.; Phomphrai, K.; Coordination Chemistry and Reactivity of Monomeric Alkoxides and Amides of Magnesium and Zinc Supported by the Diiminato Ligand CH(CMeNC<sub>6</sub>H<sub>3</sub>-2,6-<sup>i</sup>Pr<sub>2</sub>)<sub>2</sub>. A Comparative Study. *Inorg. Chem.* **2002**, *41*, 2785–2794. (b) Baker, G. J.; White, A. J. P.; Casely, I. J.; Grainger, D.; Crimmin, M. R.; Catalytic, Z-Selective, Semi-Hydrogenation of Alkynes with a Zinc–Anilide Complex. *J. Am. Chem. Soc.* **2023**, *145*, 7667–7674.
- (24) Scheiper, C.; Schulz, S.; Wölper, C.; Bläser, D.; Roll, J.; Synthesis and Single Crystal X-ray Structures of Cationic Zinc  $\beta$ -Diketiminato Complexes. *ZAAC*, **2013**, 639, 1153–1159.
- (25) Cheng, M.; Lobkovsky, E. B.; Coates, G. W.; Catalytic Reactions Involving C1 Feedstocks: New High-Activity Zn(II)-Based Catalysts for the Alternating Copolymerization of Carbon Dioxide and Epoxides. *J. Am. Chem. Soc.* **1998**, *120*, 11018–11019.
- (26) (a) Friedrich, A.; Eyselien, J.; Elsen, H.; Langer, J.; Pahl, J.; Wiesinger, M.; Harder, S.; Cationic Aluminium Complexes as Catalysts for Imine Hydrogenation. *Chem. Eur. J.* **2021**, *27*, 7756–7763. (b) Qian, B.; Ward, D. L.; Smith, M. R.; Synthesis, Structure, and Reactivity of  $\beta$ -Diketiminato Aluminum Complexes. *Organometallics* **1997**, *17*, 3070–3076.
- (27) Radzewich, C. E.; Guzei, I. A.; Jordan, R. F.; Three-Coordinate Cationic Aluminum Alkyl Complexes Incorporating  $\beta$ -Diketiminato Ligands. *J. Am. Chem. Soc.* **1999**, *121*, 8673–8674.
- (28) (a) Dagonne, S.; Bellemin-Laponnaz, S.; Welter, R.; Synthesis and Structure of Neutral and Cationic Aluminum Complexes Incorporating Bis(oxazolinato) Ligands. *Organometallics* **2004**, *23*, 3053–3061. (b) Wrobel, O.; Schaper, F.; Brintzinger, H. H.; Bulky Siloxyaluminum Alkyls as Models for Al<sub>2</sub>Me<sub>6</sub>-Treated Silica Gel Surfaces. Characterization of a Dimethylaniline-Stabilized Dimethylaluminum Cation. *Organometallics* **2004**, *23*, 900–905.
- (29) Camp, C.; Arnold, J.; On the non-innocence of “Nacnacs”: ligand-based reactivity in  $\beta$ -diketiminato supported coordination compounds. *Dalton Trans.* **2016**, *45*, 14462–14498.

- (30) Bai, G.; Wei, P.; Das, A.; Stephan, D. W. Mono- and Bimetallic (NacNac)Ni Cyclopentadienyl Complexes. *Organometallics* **2006**, *25*, 5870--5878.
- (31) Scheiper, C.; Naglav, D.; Bläser, D.; Wölper, C.; Schulz, S.; Synthesis and X-ray Crystal Structures of Zinc Dichloride Complexes Supported by a  $\beta$ -Diimine Ligand. *ZAAC*, **2015**, *641*, 871–875.
- (32) For reviews covering NacNacM species see: (a) Bourget-Merle, L.; Lappert, M. F.; Severn, J. R.; The Chemistry of  $\beta$ -Diketiminatometal Complexes. *Chem. Rev.* **2002**, *102*, 3031–3066. (b) Asay, M.; Jones, C.; Driess, M.; N-Heterocyclic Carbene Analogues with Low-Valent Group 13 and Group 14 Elements: Syntheses, Structures, and Reactivities of a New Generation of Multitalented Ligands. *Chem. Rev.* **2011**, *111*, 354–396. (c) Webster, R. L.;  $\beta$ -Diketimate complexes of the first row transition metals: applications in catalysis. *Dalton Trans.*, **2017**, *46*, 4483–4498 (d) Roy, M. M. D.; Omaña, A. A.; Wilson, A. A.S.; Hill, M. S.; Aldridge, S.; Rivard, E. Molecular Main Group Metal Hydrides. *Chem. Rev.* **2021**, *121*, 12784–12965.
- (33) (a) Han, Y.; Deng, L.; Ziegler, T.; A Density Functional Study of Hydride and Methyl Migratory Insertion in CpM(PH<sub>3</sub>)(CH<sub>2</sub>CH<sub>2</sub>)R<sup>+</sup> (M = Co, Rh, Ir; R = H, CH<sub>3</sub>). *J. Am. Chem. Soc.* **1997**, *119*, 5939–5945. (b) Koga, N, Morokuma, K, Carbonyl insertion into Pd–H bond of HPd(R)(CO)(PH<sub>3</sub>) (R = CH<sub>3</sub>, H) and comparison with that into Pd–CH<sub>3</sub> bond – an ab initio MO study. *New J. Chem.* **1991**, *15*, 749.
- (34) Note these three  $\phi$  values indicate more distortion than in the reported solid-state structure for H–NacNacZnCl<sub>2</sub> ( $\phi$  = 109°), see Ref. 31, presumably due to the greater bulk of NR<sub>3</sub> relative to chloride.



◆ Transition metal-free catalytic process ◆ Two dehydrocoupling pathways ◆ NacNac ligand non innocence

---

---